NASA Technical Memorandum 80200

A SUMMARY AND EVALUATION OF SEMI-EMPIRICAL METHODS FOR THE PREDICTION OF HELICOPTER ROTOR NOISE

ROBERT J. PEGG

DECEMBER 1979

National Aeronautics and Space Administration
Langley Research Center
Hampton, Virginia 23665

A SUMMARY AND EVALUATION OF SEMI-EMPIRICAL METHODS FOR THE PREDICTION OF HELICOPTER ROTOR NOISE

By

Robert J. Pegg

SUMMARY

A compilation and evaluation of existing semi-empirical methods for predicting various helicopter rotor noise components is given in this report. These prediction methods should be useful to preliminary design groups, planners and user/operators requiring easy-to-use techniques for the evaluation of the acoustic characteristics of helicopters.

The author has selected appropriate available theoretical methods which can be solved easily through closed-form solutions or with the help of computer analyzed graphs. Examples are included which show the use of the prediction techniques and are compared to experimental data.

INTRODUCTION

The far-field noise produced by rotors is comprised of periodic components; a series of tones occurring at the blade passage frequency and multiples thereof, and broadband components; a random noise arising from inflow from inflow turbulence and wake-shedding induced force fluctuations (see figure 1). In addition to these primary noise components, rotors can sometimes produce an impulsive type noise generally called blade slap which arises from either

blade vortex interaction or compressibility (thickness) effects or both. The complex aerodynamic flow field associated with a helicopter strongly influences noise components which are important in different portions of the flight envelope. During level flight with a low advancing tip Mach number, the rotational broadband noise can be considered as the major noise components. At high advancing tip Mach numbers, thickness and other compressibility effects can be expected to predominate. When the helicopter is flying in certain flight (particularly descent) conditions, blade-vortex interactions can occur and and may result in intense impulsive noise.

The purpose of this report is to provide a compilation of existing semi-empirical methods for predicting the various rotor noise components for given flight operating conditions. These prediction methods should be useful to preliminary design groups for parametric studies and for extrapolating to new designs; to planners who want to compare one type of operating procedure with another or want to compare the noise signatures of various helicopters for a given procedure; and to the user/operator requiring an independent evaluation of the acoustic characteristics of several helicopters.

In the text of the report, the empirical prediction procedures are described. The description includes the input and output parameter list, steps of computation, required equations and graphs, and the range of validity for each part of the prediction procedures. A section is also provided showing illustrative examples of the methodology developed in the report. The examples include calculations for rotational noise, blade/vortex interaction noise, and high-speed thickness noise.

Appendices, in which considerable attention has been devoted to the chronological development of the rotor blade noise technology, have been

included in an effort to provide the user with a greater insight into the use of the prediction methods. A diagram of the various rotor noise components is shown in figure 1. The sequence presented in this figure has been followed in the general organization of the material in both the text and the Appendices. The material in the Appendices has the additional advantage of giving the reader some insight into the reasoning for recommending certain prediction procedures and the options available to the reader if variations in the prediction methods must be considered. Two recent publications, reference 1 and 2, present helicopter noise calculation procedures which are similar to the level of prediction sophistication outlined in this report, but which are primarily graphically oriented and do not allow the calculation flexibility of this report.

SYMBOLS

A_b blade area, m^2

A_c correlation area, m^2

A_T blade tip area affected by vortex, m^2

B number of blades

c blade chord, m

c_o speed of sound at sea level standard conditions, m/sec

C_o amplitude of first load harmonic

$C_{\lambda,D}$, $C_{\lambda,T}$, $C_{\lambda,C}$, $C_{0,T}$ complex loading coefficients in the rotational noise equation (A-4)

$\bar{c}_{d_o}$ incremental blade drag coefficient

D rotor diameter, m

D. L. rotor disk loading, n/m^2

$\bar{C}_L$ mean lift coefficient

E	number of interactions per revolution
f	frequency, Hz
f_p	peak frequency, Hz
F	point force
h	blade thickness, m
J	summation limit in compressibility noise equation
J_{mB}	Bessel function
k	$= \frac{c}{2R}$
K_T	thrust constant, N/m^2
K_1	turbulent boundary layer area correlation constant
ℓ_c	correlation length, m
L_o	blade lift, Newton
m	sound pressure harmonic number
M_{dd}	drag divergence Mach number
M_e	effective Mach number $= \frac{M_T + M_F \sin\psi}{1 - M_F \cos\beta}$
M_F	forward velocity Mach number
M_r	component of the relative Mach number in observer direction
M_t	blade tip Mach number
n	loading fall-off exponent
N	rotational speed, rev/sec
P	power, watts
P_m	complex sound pressure due to the first Λ loading harmonic, N/m^2
P_{m_c}	sound pressure due to high frequency in plane loads, N/m^2
P_{m_D}	sound pressure due to high frequency drag loads, N/m^2

p_{m_T}	sound pressure due to high frequency thrust loads, N/m^2
q	dynamic head, N/m^2
r	distance from source to observer, m
R	rotor radius, m
R_e	effective blade radius - xR, m
RN	Reynolds Number
$S_{1/3}$	normalized broadband noise spectrum
t	time, sec
T	total system thrust, Newton
u	gust magnitude, m/sec
U	freestream total velocity, m/sec
V	forward velocity, m/sec
V_d	descent velocity, m/sec
V_T	blade tip speed, m/sec
w	rotor induced velocity in forward flight, m/sec
w_o	rotor induced velocity in hover, m/sec
W	total acoustic power, watts
x	fraction of radius at which rotor forces are assumed to act
x_i, y_i	observer source location coordinates
α	angle between flight path and rotor disk plane, deg.
β	observer angle measured from the rotor disk plane, deg
χ_s	blade loading spectrum function
δ^*	boundary layer thickness
ΔL	incremental blade lift due to vortex interactions, Newton
ΔSPL_{bv}	blade-vortex interaction noise component sound pressure level

ΔSPL_c normalized compressibility-induced profile drag noise component sound pressure level

ΔSPL_K normalized thickness noise sound pressure level correction factor

ΔSPL_{mr} normalized main rotor noise component sound pressure level

ΔSPL_T normalized thickness noise component sound pressure level

ΔSPL_{tr} normalized tail rotor noise component sound pressure level

$\Delta\psi$ azimuth portion of disk within which blade vortex interaction occurs, deg

γ angle between flight path and horizontal, deg

λ loading harmonic number

Λ summation limit in equation (A-4)

ω sinusoidal gust frequency, rad/sec

ψ rotor azimuth angle, deg

ψ_o complete rotor azimuth of 360°

σ_w load solidity

θ_1 angle between negative thrust axis and line from hub to observer, deg.

RECOMMENDED SEMI-EMPIRICAL PREDICTION PROCEDURES

The background for prediction techniques of helicopter rotor noise components identified in figure 1 has been detailed in the Appendices. Only the steps necessary for computation are described in this section. These prediction techniques are, in some cases, semi-empirical which allows their use for the fast calculation of helicopter rotor noise but which may limit their universal applicability. Some degree of engineering insight is necessary to adequately utilize these procedures. Several examples are given in the

following section illustrating the use of the equations and showing the correlation with measured noise levels where possible.

Periodic Noise

Rotational noise/steady and unsteady loading.- The recommended procedure for calculating the rotational noise of a helicopter is the one developed by Lowson and Ollerhead (ref. 3). The procedure does not predict the discrete noise generated by blade thickness or blade/vortex interaction. This method is based on an arbitrary point loading with random phasing and an assumed ratio of thrust to drag to radial force of 10:1:1. These force ratios are, in reality, varying with forward speed, configuration changes, etc. The unsteady load on the rotor is represented by a spectrum of loading harmonics in the computation of Lowson and Ollerhead. In the high frequency range, the loading harmonics are assumed to decay with an exponent of n = -1.85. This is a representative value based on the work shown in references 3 and 4. The prediction procedure is given as follows.

Input parameters:

B	number of blades
m	acoustic harmonic number
M_F	forward velocity of helicopter
M_t	blade tip Mach number
N	rotor speed; rev/sec
r	distance from souce to observer
R	rotor radius
R_e	effective rotor radius
T	total rotor thrust

β observer angle measured from rotor disk

ψ rotor azimuth angle

Output parameters:

f frequency at a given acoustic harmonic number

SPL_{mB} sound pressure level at a given harmonic number

Computational Procedure:

Step 1. Compute the effective rotor tip Mach number by using:

$$M_e = \frac{M_t + M_F \sin\psi}{1 - M_F \cos\beta} \tag{1}$$

Step 2. Compute the blade passage frequencies according to:

$$f = \frac{mBN}{1 - M_F \cos\beta} \tag{2}$$

Step 3. Determine ΔSPL_{mr} from figure 2 according to the value of M_e and β. The value of the last two parameters must be within the range of

$$0.5 \leq M_e \leq 0.9 \quad ; \quad 0. \leq \beta \leq 80.$$

Figure 2 is obtained from reference 3.

Step 4. Compute the sound pressure level SPL_{mB} for each value of mB by using:

$$SPL_{mB} = 20 \log \frac{R_e}{r} + 20 \log \frac{T}{\rho c_o^2 R^2} + \Delta SPL_{mr} \tag{3}$$

This procedure can also be used to calculate the rotational noise of a tail rotor. Because of the complicated flow environment in which the tail rotor normally operates, a different set of incremental sound

pressure levels, ΔSPL_{tr}, should be determined in Step 3 using values of ΔSPL_{tr} provided in figure 3. These values are based on an assumed ratio of thrust to drag to radial forces of 10:1:0 and a loading exponent $n = -2.1$. Figure 3 applies for the tail rotor of a hovering helicopter. According to reference 5, a high frequency loading exponent n of approximately -1.85 can be used for inflight tail rotor rotational noise. Hence, figure 2 may be used for these latter cases. The difference in the assumed values of thrust to drag to radial force ratios between figures 2 and 3 should be noted in practical applications.

Rotational noise/compressibility-induced profile drag noise.- This noise source is attributed to periodically fluctuating torque loads on a helicopter rotor blade generally occurring in high-speed forward flight. The simplified prediction procedure presented here is based on the work of Arndt and Borgman (ref. 6).

Input parameters:

c	rotor blade chord length
M_e	effective blade tip Mach number
M_{dd}	drag divergence Mach number
r	distance from source to observer
R	rotor radius
R_e	effective rotor radius
β	observer angle measured from the rotor disk

Output parameters:

SPL_{mB}	component sound pressure level at given blade harmonic frequency

Computational Procedure:

Step 1. The effective tip Mach number is obtained according to equation (1). If M_e is less than or equal to M_{dd}, the compressibility-induced profile drag noise components vanishes. Proceed with Steps 2 and 3 if M_e is greater than M_{dd}.

Step 2. Determine ΔSPL_c from figure 4 by using values of mB, M_e, and β. The range of M_e is restricted to

$$M_{dd} \leq M_e \leq 0.95 \quad .$$

Step 3. Compute the compressibility-induced profile drag noise component by using the following equation:

$$SPL_{mB} = 20 \log \frac{R_e}{r} + 20 \log [(M_e - M_{dd})\, c/R] + \Delta SPL_c - 21.6 \qquad (4)$$

Thickness noise.- The method chosen here for the computation of helicopter blade thickness noise was developed by Hawkings and Lowson (ref. 7).

Input parameters:

B	number of blades
c	blade chord length
h	blade thickness
M_e	effective tip Mach number
r	distance from source to observer
R	rotor radius
β	observer angle measured from the rotor disk

Output parameter:

SPL_{mB}	sound pressure level at a given harmonic frequency.

Computational procedure:

Step 1. Determine ΔSPL_T from figure 5 according to given values of mB, M_e, and β. The range of M_e is confined to

$$0.8 \leq M_e \leq 0.95 \quad .$$

Step 2. Determine ΔSPL_K from figure 6 according to the harmonic number mB and the blade chord to rotor diameter ratio, c/D.

Step 3. Compute the sound pressure level for the thickness noise component by using the following equation:

$$SPL_{mB} = 40 \log M_e + 20 \log R/r + 20 \log h/c + 20 \log B + \Delta SPL_T + \Delta SPL_K - .9 \tag{5}$$

In this computational procedure, the curves in figure 5 are computed according to the Hawkings and Lowson theory with a value of $c/D = 0.03$. The incremental sound pressure level adjustment ΔSPL_K is a correction factor for rotors having different c/D values. This correction factor is assumed to be independent of observer angle.

Interaction noise/blade and vortex interaction.- The computation of noise resulting from the interaction of a helicopter rotor blade and a trailing tip vortex is based on the work of Wright (ref. 8). This noise mechanism is present only for some helicopter flight conditions. Figure 7 illustrates an example of helicopter flight conditions where the wake trajectories interact with the rotor blades to produce the impulsive noise which is typical of this noise component.

Input parameters:

B	number of blades
L_o	average blade lift

N	rotor speed, rev/sec
r	distance from source to observer
T	total thrust of rotor
β	observer angle measured from rotor disk
ΔL	incremental lift on blade owing to interaction
ψ_o	total disk azimuth angle, 360°
ρ	air density

Output parameter:

SPL_{mB}	sound pressure level at given harmonic frequency

Computational procedure:

Step 1. Determine ΔSPL_{bv} from figure 8 for given values of m, B and $\Delta\psi/\psi_o$. The range of the aximuth ratio given in figure 8 is

$$0.02 \leq \Delta\psi/\psi_o \leq 0.05 \quad .$$

Step 2. Compute the sound pressure level for the blade-vortex interaction noise by using the following equation:

$$SPL_{mB} = 20 \log \left(\frac{\Delta L}{L_o} \cos\beta\right) + 20 \log \frac{T \cdot N}{\rho c_o^3 r} + \Delta SPL_{bv} + 190.2 \qquad (6)$$

It has been found from experience that for the noise resulting from a blade-vortex interaction on the advancing side of the rotor disk, a typical value of the azimuth ratio $\Delta\psi/\psi_o$ is 0.05. The lift ratio $\Delta L/L_o$ varies from about .15 for a conventional blade (constant chord, linear twist, square tip) to about .07 for a blade with blade tip air injection. In the present computational procedure, values of the azimuth ratio and the incremental lift ratio are empirically determined.

Interaction noise/installation effect.- Increased attention is being directed at subject of noise generated by the interaction of a turbulent airstream with a lifting rotor. There are currently no verified procedures available for the calculation of helicopter installation noise.

Broadband Noise

Broadband noise is a complex noise source comprised of a number of different components. Current prediction techniques for boundary layer, turbulent inflow, and vortex interaction effects need additional investigation to provide reasonable correlation with experimental data. The recommended prediction procedure is based on a dimensional analysis approach. Contributions from various components, as shown in figure 1, are not explicitly identified in this prediction procedure.

The recommended rotor-generated broadband noise computation procedure is based on the work of Lowson (ref. 9), Hubbard (ref. 10), Schlegel (ref. 11), and Munch (ref. 12).

Input parameters:

A_b	total blade area of the rotor
$\bar{C}_L$	average blade lift coefficient
T	total thrust of the rotor
V_T	rotor tip speed
r	distance from source to observer
θ_1	angle between negative thrust axis and line from hub to observer, deg.

Output parameter:

$SPL_{1/3}$ one-third-octave band sound pressure level for the overall contribution from all broadband noise components.

Computational procedure:

Step 1. Compute the peak broadband noise frequency by using the following equation*:

$$f_p = -240 \log T + 2.448 V_T + 942 \tag{7}$$

Step 2. Identify the peak frequency with a standard 1/3-octave band.

Step 3. Compute the peak 1/3-octave band sound pressure level by using the following equation:

$$SPL_{1/3} = 20 \log \left(\frac{V_T}{c_o}\right)^3 + 10 \log \frac{A_b}{r^2} (\cos^2 \theta_1 + .1) + S_{1/3} + f(\bar{C}_L) + 130 \tag{8}$$

where $S_{1/3}$ can be determined from figure 9. The lift coefficient function, $f(\bar{C}_L)$, for most helicopters with $\bar{C}_L \leq .48$ is 10 log $(\bar{C}_L/.4)$. Preliminary experimental data indicate significantly higher values of $f(\bar{C}_L)$ for $\bar{C}_L > .48$. The normalized spectrum function $S_{1/3}$ as shown in figure 9 is developed by Schlegel (ref. 11).

Step 4. Compute the sound pressure level for all the other one-third-octave bands according to equation (8) and figure 9.

---

*This equation is dimensionally incorrect and it is unit dependent. For the English system of units this equation should read:

$$f_p = -240 \log T + .746 V_T + 786 .$$

APPLICATION AND EVALUATION

This section of the report illustrates the use of the recommended prediction methods by numerical examples. In addition, an indication of parameter sensitivity and the effect of variation in any empiricism are investigated. The examples chosen represent a wide range of operating conditions and variables. The particular examples show how to apply the prediction techniques and the corresponding agreement with existing experimental data. The first example specifically illustrates the calculation of rotational noise from the main and tail rotors of a large hovering transport-type helicopter. The second example illustrates the prediction of impulsive noise resulting from blade/vortex interaction for a wind-tunnel model in a simulated rate of descent. The calculation of high-speed impulsive noise is illustrated in the third example and compared with experimental wind-tunnel model data.

Example 1

The noise from a large, hovering, single-main-rotor helicopter can be calculated using equations (2), (3), (7), and (8). Only rotational and broadband noise components are considered for this example because the tip speed is sufficiently low so that thickness and compressibility noise do not affect the acoustic spectra. Since the helicopter is hovering no blade/vortex interaction is assumed to occur. For the conventional type helicopter, this procedure must also be repeated for the tail rotor and the results superimposed on a frequency basis. The following information is required to predict the noise:

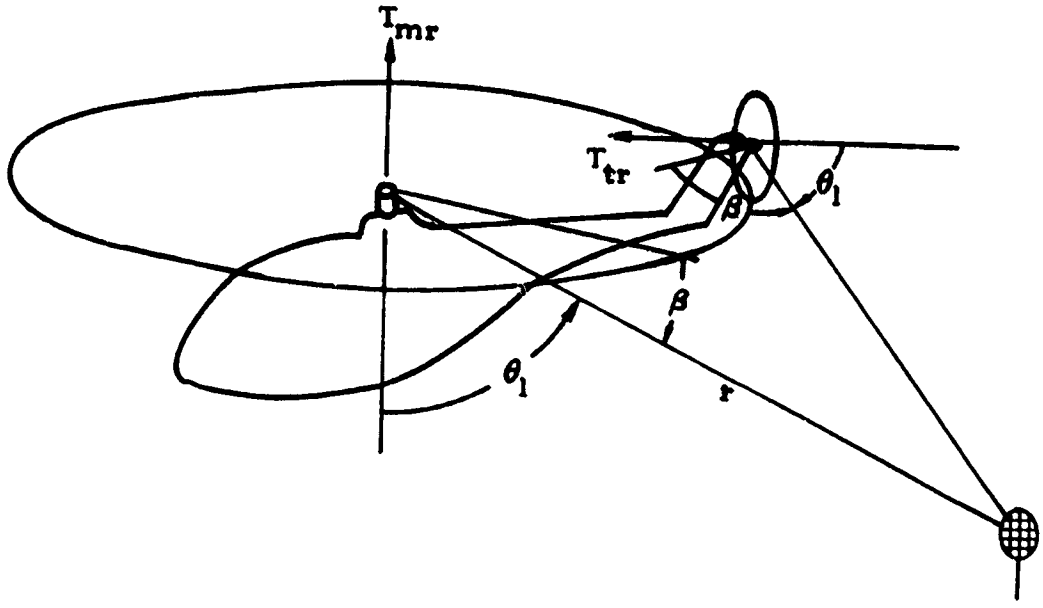

	Main Rotor	Tail Rotor
Tip Mach number	.6	.6
Rotor speed, rps	3.5	21.1
Blade radius, m	9.45 (31 ft)	1.52 (5 ft)
Observer angle, β, deg	5°	80°
Number of blades	5	5
Thrust, N	69420 (15,600 lbs)	5206 (1,170 lbs)
Blade area, m^2	18.58 (200 ft^2)	3.44 (37 ft^2)
Air density, kg/m^3	1.228 (.00238 $slug/ft^3$)	1.228 (.00238 $slug/ft^3$)
Observer distance, m	61.6 (202 ft)	62.2 (204 ft)
Mean lift coefficient	.438	.182

The tail rotor rotational noise and thrust is based on the assumption that the ratio of rotor blade thrust to drag is 10:1 and that the distance from the tail rotor to main rotor is 11.1 m. The radius and Mach number

at which the rotor forces are assumed to be concentrated is .9 of the actual radius.

The rotor noise for the example hovering helicopter is composed of both rotational and broadband components for the two rotors. The rotational noise is calculated first from equation (3) and figure 2. Values of the tip Mach number are obtained by interpolation in figure 2.

$$\underline{\text{Rotational}}: = 20 \log \frac{8.50}{61.6} + 20 \log \frac{69420}{(1.228)(344)^2(9.45)^2} + \Delta SPL_{mr}$$

$$= 17.2 - 45.4 + \Delta SPL_{mr}$$

$$= -62.6 + \Delta SPL_{mr}$$

$$\text{fundamental frequency} = \frac{NB}{(1 - M_F \cos\theta)} = 17.5 \text{ Hz}$$

mB	Frequency	ΔSPL_{mr} *	Calculated, SPL_{mB}	Experimental, SPL_{mB} **
5	17.5	148.4	85.7	85.0
10	35.0	143.5	80.8	79.5
15	52.5	140.2	77.5	76.0
20	70.0	138.4	75.7	73.0

* From figure 3 for $M_e = .54$ and $\beta = 80°$

** Data from reference 13, figure 17.

Tail rotor: $= 20 \log \frac{1.37}{62.2} + 20 \log \frac{5206}{(1.228)(344)^2(1.52)^2} + \Delta SPL_{tr}$

$= -33.1 - 36.2 + \Delta SPL_{tr}$

$= -69.3 + \Delta SPL_{tr}$

fundamental frequency $= \frac{(5)(21.1)}{1-(0)\cos 80} = 105.5$ Hz;

mB	frequency	ΔSPL_{tr}*	Calculated, SPL_{mB}	Experimental SPL_{mB}**
5	105	154.4	85.1	82
10	210	149.2	79.9	76
15	315	145.9	76.6	75
20	420	143.8	74.5	73

*From figure 3 for $M_e = .54$ and $\beta = 80°$.

**Data from reference 13, figure 17.

Broadband:

The rotor broadband noise is calculated based on equation (8). For the main rotor:

$$SPL_{1/3} = 20 \log \left(\frac{208}{344}\right)^3 + 10 \log \left[\frac{18.6}{(61.6)^2}(\cos^2 85 + .1)\right] + S_{1/3} + 10 \log \left(\frac{.438}{.4}\right) + 130.$$

$$= -13.1 - 32.8 + S_{1/3} + .39 + 130.$$

$$= 84.5 + S_{1/3}$$

For the tail rotor:

$$SPL_{1/3} = 20 \log \left(\frac{202}{344}\right)^3 + 10 \log \left[\frac{3.44}{(62.2)^2} (\cos^2 10 + .1)\right] + S_{1/3} +$$

$$+ 10 \log \left(\frac{.182}{.4}\right) + 130$$

$$= -13.9 - 30.2 + S_{1/3} - 3.42 + 130.$$

$$= 82.5 + S_{1/3}$$

The spectrum correction value, $S_{1/3}$, is obtained from figure 9. Peak frequencies for both main and tail rotors are calculated from equation (7):

$$f_p = -240 \log (69420) + 2.448(208) + 942$$

$$= -1162 + 509 + 942 = 289 \text{ Hz}$$

$$f_p = -240 \log (5206.5) + 2.448(202) + 942$$

$$= -892 + 494 + 942 = 544 \text{ Hz}$$

The third octave frequency spectra for the broadband noise uses the above information and is calculated below for both the main and tail rotors. The main rotor broadband peak frequency of 289 Hz falls within a band where the center frequency is 315 Hz, therefore:

1/3 Octave Center Freq.	$S_{1/3}$	$SPL_{1/3}$
40	-19.5	64.8
80	-15.3	69.0
160	-11.7	72.6
315	- 7.5	76.8
630	-11.5	72.8
1,250	-12.1	72.2
2,500	-16.5	67.8
5,000	-17.0	67.3
10,000	-21.8	62.5

Tail rotor peak frequency, f_p = 544 Hz, lies in a third octave band with a center frequency of 630 Hz, therefore:

1/3 Octave Center Freq.	$S_{1/3}$	$SPL_{1/3}$
20	-29.0	56.1
40	-24.5	58.6
80	-19.5	63.6
160	-15.3	67.8
315	-11.7	71.4
630	- 7.5	75.6
1,250	-11.5	71.6
2,500	-12.1	71.0
5,000	-16.5	66.6
10,000	-17.0	66.1

Discrete noise components at blade passage frequencies previously calculated may be combined with the one-third-octave broadband noise levels by adding the sound pressure levels in each 1/3-octave band. The calculated values are then combined and shown in the following summary table. The table is carried out to a frequency where most discrete data for conventional helicopters become less than the broadband noise.

1/3-Octave Center Freq	Tail rotor, SPL		Main rotor, SPL		Total, SPL	Exp. Total (Ref. 13)
	Rot.	B. B.	Rot.	B. B.		
16			85.7		85.7	85
20		54.1			54.1	
25						
31.5			80.8		80.8	79.5
40		58.6		64.8	66.5	
50			77.5		77.5	76
63			75.7		75.7	
80		63.6		69.0	70.1	73
100	85.1				85.1	82
125						
160		67.8		72.6	73.8	
200	79.9				79.9	76
250						
315	76.6	71.4		76.8	80.3	75
400	74.5				74.5	73
500						
630		75.6		72.8	77.4	
800						
1 K						
1.25 K		71.6		72.2	74.9	
1.6 K						
2 K						
2.5 K		71.0		67.8	72.7	

Correlation of the calculated sound pressure levels and those flight test measurements in reference 13 indicate good agreement to the fourth harmonic for both the main and tail rotors.

A sensitivity analysis of specific parameters in the rotational and broadband noise components for the previous example that are difficult to measure experimentally indicates that a 10 percent variation in: a) thrust will

result in approximately .9 dB change in noise level and 10 Hz shift in broadband frequency; b) air density will change the level approximately .9 dB; c) speed of sound will change the level approximately 1.8 dB and; d) rotor speed will change the broadband level approximately 2.8 dB and shift the center frequency 50 Hz.

Example II

This example illustrates the use of the blade-vortex interaction equation (eq. (6)), as applied to a two-bladed rotor wind-tunnel model. The experimental data used for correlation in this example are reported in reference 14. The contribution from the rotational and thickness noise components is not affected by the periodic loading noise induced by the blade/vortex interaction and is therefore not considered in this example. The necessary parameters required to determine the discrete harmonics resulting from a blade/vortex interaction and the specific values for the example are listed below:

Total rotor thrust, N	458.35	(103 lb)
Tip Mach number	.433	
Rotor speed, rps	22.75	
Observer angle, deg	49°	
Observer distance, m	1.02	(3.35 ft)
Forward speed, m/sec	21.3	(70 ft/sec)
Speed of sound, m/sec	344.	(1130 ft/sec)

It is assumed that the major contribution of the interaction occurs over that portion of the azimuth which starts when the vortex first intercepts the tip of the blade and the blade sweeps through approximately 18°. The momentary blade load disturbance, ΔL, caused by this interaction is assumed to be

20 percent of the load of one blade or 10.3 lb. The rms sound pressure harmonic levels from equation (6) and figure 8 are therefore

$$SPL_{mB} = 20 \log (.2 \cos 49) + 20 \log \frac{(458.35)(22.75)}{(1.228)(344)^3(1.02)} + \Delta SPL_{bv} + 190.2$$

$$= -17.6 - 73.8 + \Delta SPL_{bv} + 190.2$$

$$= 98.8 + \Delta SPL_{bv}$$

mB	frequency, Hz	ΔSPL_{bv}*	SPL_{mB}, dB (from eq (5))
4	228	-23.0	75.8
10	455	-11.5	87.3
16	683	- 6.0	92.8
20	910	- 3.0	95.8
24	1138	- 1.7	97.1
30	1365	- 2.3	96.5
36	1593	- 4.5	94.3
40	1820	- 9.5	89.3
44	2048	-22.3	76.3

* From figure 8, $\frac{\Delta\psi}{\psi_o} = .05$

These calculated harmonics make up an envelope and are superimposed on the experimental data taken from reference 14 and shown in figure 10. The agreement shown in this figure between theory and measured data is good, that is, the harmonic levels and characteristic spectrum shape are similar.

The harmonic content occurring at the lowest blade passage frequencies is due to the steady rotational and blade thickness sources. The periodic force fluctuation caused by the blade/vortex interactions do not affect these harmonics.

Example III

This example illustrates the prediction and correlation of the high tip-speed noise sources. Experimental data for this example are taken from reference 15. These data were taken from a hovering 1/7-scale UH-1 rotor operating at two thrust conditions. Comparisons of the calculated results and the experimental data are given in figure 11 for two tip Mach numbers. The following information is required for the calculations:

$B = 2$

$r = 3.14$ m (10.3 ft)

$\beta = 0°$

$T = 485$ N, 676 N (109 lb, 152 lb)

$M_e = .9$ ($N = 47.2$ rps, $f_o = 94$ Hz)

$M_e = .8$ ($N = 41.95$ rps, $f_o = 84$ Hz)

$c = .0762$ m (.25 ft)

$R = 1.05$ m (3.43 ft)

$M_{dd} = .8$ (fig. 15)

$h/c = .12$

$R_e = .945$ m (3.09 ft)

Numerical calculations will be made to compute compressibility noise, rotational noise and finally the contribution of thickness noise. These calculations are then compared with the measured data. The compressibility-induced profile drag noise is determined from equation (4) and figure 4 for $M_e = .9$:

$$SPL = 20 \log \frac{.934}{3.14} + 20 \log [(.9 - .8)\ .0762/1.05] + \Delta SPL_c - 21.6$$

$$= -10.4 - 42.8 - 21.6 + \Delta SPL_c = 74.8 + \Delta SPL_c$$

mb	frequency, Hz	ΔSPL_c	SPL_{mB}, dB (from eq. (3))
2	94	173.9	99.1
4	188	175.3	100.5
8	376	176	101.2
12	564	175.7	100.9
16	752	174.9	100.1
20	940	173.9	99.1
30	1410	170.2	95.4

These values are shown in the lower portion of figure 11 as the square data points.

The compressibility-induced drag noise calculated values for M = .8 are zero because the tip Mach number is equal to the drag divergence Mach number.

Thickness noise values are similarly determined from equation (5) and figures 5 and 6.

$$SPL_{mB} = 40 \log (.9) + 20 \log \left(\frac{1.05}{3.14}\right) + 20 \log (.12) + 20 \log (2) +$$

$$+\Delta SPL_T + \Delta SPL_K - .9$$

$$= -24.6 + \Delta SPL_T + \Delta SPL_K \quad (M_e = .9)$$

$$= -26.7 + \Delta SPL_T + \Delta SPL_K \quad (M_e = .8)$$

mB	freq. Hz	ΔSPL_K (for M=.8 & .9)	$\Delta SPL_T @ M_T=.8$	SPL,dB	$\Delta SPL_T @ M_T=.9$	SPL,dB
2	94	3.5	117.9	94.7	119.6	98.4
4	188	3.5	122.1	99.6	119.6	104.1
8	386	3.4	123.9	100.6	129.7	108.4
12	564	3.2	123.2	99.7	131.6	110.1
16	752	3.1	121.7	98.1	132.4	110.8
20	940	3.0	119.6	95.9	132.7	111.0
30	1410	2.5	113.4	89.2	132.2	110.0

The rotor is producing thrust and therefore a rotational noise is also calculated. This is done using equation (3) and figure 2 for an effective tip Mach number of .72 and .81 (Mach number at assumed force location .9R):

$$SPL_{mB} = 20 \log \frac{(.945)}{3.14} + 20 \log \frac{485}{(1.228)(344)^2(1.05)^2} + \Delta SPL_{mr}$$

$$= -10.4 - 50.4 + \Delta SPL_{mr} = -60.8 + \Delta SPL_{mr}$$

mB	freq. Hz	$\Delta SPL_{mr} @ M_e=.81$	SPL_{mB},dB (from eq. (2))	$\Delta SPL_{mr} @ M_e=.72$	SPL_{mB},dB (from eq.(2))
2	94	155.5	94.7	154.3	93.5
4	188	156.7	95.9	154.2	93.4
8	376	157.3	96.5	153.3	92.5
12	564	156.6	95.8	150.6	89.8
16	752	155.5	94.7	147.7	86.9
20	940	154.5	98.7	145.9	85.1
30	1410	152.4	91.6	142.3	81.5

The summation of the three noise component levels for this rotor are listed below:

mB	frequency, Hz	SPL @ M_T = .8	SPL @ M_T = .9
2	94	97.2	102.6
4	188	100.5	106.1
8	376	101.2	109.4
12	564	100.1	110.7
16	752	98.4	111.3
20	940	96.3	111.4
30	1410	89.9	110.2

These calculated results are compared with the experimental data of reference 15. The calculated acoustic spectrum shapes, shown as envelopes in figure 11, are very similar to the experimental spectrum shapes and the individual harmonic levels are generally within 3 - 8 decibels of the measured values. Some of the differences between the calculated and measured values in figure 11 can be attributed to the fact that the experimental rotor had a NACA 0012 airfoil section (blunt leading edge) whereas the thickness noise calculations are made using a circular arc airfoil (sharp leading edge) for ease of analysis.

From figure 11, it can be seen that the primary noise component is that from thickness noise. Compressibility and rotational noise fall off more rapidly with increasing harmonic number. A ten percent variation in tip Mach number will vary the predominant thickness noise harmonic terms approximately 1.7 dB.

CONCLUDING REMARKS

Semi-empirical methods for the calculation of helicopter main- and tail-rotor noise have been presented. These methods represent, in the author's opinion, the state of the art for semi-empirical helicopter noise prediction. The methods have been presented in such a way that solutions can be obtained with the help of computer-derived graphs. Examples have been provided illustrating both the analysis procedure and the degree of agreement with experimental results. Agreement of the analytical and experimental results is generally good. The calculation procedures have been organized so that as improvements are made, they can be easily incorporated in the general calculation procedures.

REFERENCES

1. Sternfeld, Harry, Jr.; and Wiedersum, Carl W.: Study of Design Constraints on Helicopter Noise. NASA CR 159118, July 1979.

2. Magliozzi, Bernard: V/STOL Rotary Propulsion Systems Noise Prediction and Reduction. U. S. Dept. of Transportation. No. FAA-RD-76-49, May 1976.

3. Lowson, M. V.; and Ollerhead, J. B.: Studies of Helicopter Rotor Noise. USAAVLABS Tech. Report No. 68-60, January 1969.

4. Kasper, Peter K.: Determination of Rotor Harmonic Blade Loads from Acoustic Measurements. NASA CR 2580, Oct. 1975.

5. Levine, Larry S.: An Analytic Investigation of Te chniques to Reduce Tail Rotor Noise. NASA CR 145014, July 1976.

6. Arndt, Rodger E. A.; and Bergman, Dean C.: Noise Radiation from Helicopter Rotors Operating at High Tip Mach Number. American Helicopter Society, 26th Annual Forum, June 1970.

7. Hawkings, D. L.; and Lowson, M. V.: Tone Noise of High Speed Rotors. Second Aero-Acoustics Conf., Hampton, VA, March 24-26, 1975, AIAA Paper 75-450.

8. Wright, S. E.: Discrete Radiation from Rotating Periodic Sources. J. Sound and Vibration (1971) 17(4), pp. 437-498.

9. Lowson, M. V.: Thoughts on Broad Band Noise Radiation by a Helicopter. Wyle Laboratories WR 68-20, 1968.

10. Hubbard, H. H.: Propeller-Noise Charts for Transport Airplanes. NACA TN 2968,

11. Schlegel, Ronald G.; King, Robert J.; and Mull, Harold: Helicopter Rotor Noise Generation and Propagation. USAAVLABS Tech. Report No. 66-4, Oct. 1966.

12. Munch, C. L.: Prediction of V/STOL Noise for Applications to Community Noise Exposure. DOT-TSC-OST-73-19, May 1973.

13. Pegg, Robert J.; Henderson, Herbert R.; and Hilton, David A.: Results of the Flight Noise Measurement Programs Using a Standard and Modified SH-3A Helicopter. NASA TN D-7330, Dec. 1973.

14. Pegg, R. J.; and White, Richard A., Jr.: Some Measured and Calculated Effects of a Tip Vortex Modification Device on Impulsive Noise. AIAA Fourth Aero-acoustic Conf., Atlanta, GA, AIAA Paper No. 77-1341, 1977.

15. Boxwell, D. A., Yu, Y. H.; and Schmitz, F. H.: Hovering Impulsive Noise - Some Measured and Calculated Results. NASA CP 2052, Pt. 1, May 1978.

16. Lynam, E. J.; and Webb, H. A.: The Emission of Sound by Airscrews. Aeronautical Research Council, R&M 624, March 1919.

17. Bryan, G. H.: The Acoustics of Moving Sources with Application to Airscews. Aeronautical Research Council, R&M 684, 1920.

18. Gutin, L. J.: On the Sound Field of a Rotating Propeller. NACA TM 1195, 1958.

19. King, Robert J.; and Schlegel, Ronald G.: Prediction Methods and Trends for Helicopter Rotor Noise. CAL/AVLABS Third Annual Symposium, June 18-20, 1969.

20. Hubbard, Harvey H.; and Regier, A. A.: Free-Space Oscillating Pressures Near the Tips of Rotating Propellers. NACA TR 996, 1950.

21. Garrick, I. E.; and Watkins, C. E.: A Theoretical Study of the Effects of Forward Speed on the Free-Space Sound-Pressure Field Around Propellers. NACA TR 1198, 1953.

22. Watkins, C. E.; and Durling, B. J.: A Method for Calculation of Free-Space Sound Pressures Near a Propeller in Flight, Including Consideration of the Chordwise Loading. NACA TN 3809, 1956.

23. Hosier, R. N.; and Ramakrishnan, Ramani: Helicopter Rotor Rotational Noise Predictions Based on Measured High-Frequency Loads. NASA TN D-7624, Dec. 1974.

24. Sadler, S. Gene: and Loewy, Robert G.: A Theory for Predicting the Rotational and Vortex Noise of Lifting Rotors in Hover and Forward Flight. NASA CR 1333, May 1969.

25. Wright, S. E.: Sound Radiation from a Lifting Rotor Generated by Asymmetric Disk Loading. J. Sound and Vibration (1969), 9(2), p. 223-240.

26. Lowson, M. W.: The Sound Field for Singularities in Motion. Proceedings of the Royal Society, A. vol. 286, 1965.

27. Lowson, M. W.; and Ollerhead, J. B.: A Theoretical Study of Helicopter Rotor Noise. J. Sound Vibration, 9(2), pp. 197-222, (1969).

28. Sternfeld, Harry et al: An Investigation of Noise Generation on a Hovering Rotor, Part II. Boeing Company-Vertol Division.

29. Lawton, B. W.: Subjective Assessment of Simulated Helicopter-Blade-Slap Noise. NASA TN D-8359, Dec. 1976.

30. Leverton, John W.: Helicopter Noise - Are Existing Methods Adequate for Rating Annoyance or Loudness? American Helicopter Society J., vol. 19, no. 2, April 1974.

31. Cox, C. R.: Rotor Noise Measurements in Wind Tunnels. Proceedings Third CAL/AVLABS Symposium, Aerodynamics of Rotary Wind and V/STOL Aircraft, vol. 1, June 18-20, 1969.

32. Powell, Clemens A.: A Subjective Field Study of Helicopter Blade-Slap Noise. NASA TM 78758, July 1978.

33. Leverton, John W.; Southwood, B. J.; and Pike, A. C.: Rating Helicopter Noise. Helicopter Acoustics, NASA Conference Publications 2052, Pt. II, May 1978.

34. d'Ambra, F. and Daunongeot, A.: Annoyance of Helicopter Impulsive Noise. Helicopter Acoustics, NASA Conference Publication 2052, Pt. ii, May 1978.

35. Sakowski, P. C.; and Charles B. D.: Noise Measurement Test Results for AH-LG Operational Loads Survey. NASA CR 159036, June 1979.

36. Ernsthausen, E. W.: The Source of Propeller Noise. NACA TN 825, May 1937.

37. Ernsthausen, E. W.: Influence of Aerodynamic Characteristics on Sound-Blade and Radiating Power of an Aircraft. Akusticshe Zeitserrift, vol. 6, pp. 244-262.

38. Deming, A. F.: Noise from Propellers with Symmetrical Sections at Zero Blade Angle. NACA TN 605, July 1937.

39. Diprose, K. V.: Some Propeller Noise Calculations Showing the Effect of Thickness and Planform. Technical Note No. MS 19, Royal Aircraft Establishment, England.

40. Billing, H.: Modern Aeronautical Acoustics. AVA Monographs R., MAP Volkenrode Reports and Translations No. 960, July 1947.

41. Arnoldi, R. A.: Propeller Noise Caused by Blade Thickness. Report R-0896-1, United Aircraft Corporation, Jan. 1956.

42. Farassat, F.: The Acoustic Far-Field of Rigid Bodies in Arbitrary Motion, J. Sound and Vibration, vol. 32, p. 387-402, 1974.

43. Landgrebe, Anton J.: The Wake Geometry of a Hovering Helicopter Rotor and Its Influence on Rotor Performance. 28th Annual National Forum of the American Helicopter Society, May 1972.

44. Sadler, S. Gene: Development and Application of a Method for Predicting Rotor Free Wake Positions Rotor Free Wake Positions and Resulting Rotor Blade Air Loads. Vol. 1 - Model and Results. NASA CR 1911, Dec. 1971.

45. Johnson, H. Kevin: Development of an Improved Design Tool for Predicting and Simulating Helicopter Rotor Noise. USAAMRDL Tech. Report No. 74-37, June 1974.

46. Halwes, Dennis: Flight Operations to Minimize Helicopter Noise Joint Symposium on Environment Effects on VTOL Designs. AHS, AIAA, U. of Texas, Nov. 1970, Preprint No. SW-70-7.

47. Heyson, Harry H.: Nomagraphic Solution of the Momentum Equation for VTOL-STOL Aircraft. NASA TN D-814, April 1961.

48. Leverton, John W.: Helicopter Noise-Blade Slap. Pt. 1 Review and Theoretical Study. NASA CR 1221, October 1968.

49. Widnall, Sheila: Helicopter Noise Data Due to Blade-Vortex Interaction. J. Acoustical Society of America, vol. 50, no. 1, (Part II), 1971.

50. Padakannaya, Raghuveera: The Vortex Lattice Methods for the Rotor-Vortex Interaction Problem. NASA CR 2421, July 1974.

51. Filotas, L. T.: Vortex Induced Helicopter Blade Loads and Noise. J. Sound and Vibration, vol. 27, no. 3, 1973.

52. Tangler, James L.; Wohlfeld, R. M.; and Miley, Stan T.: An Experimental Investigation of Vortex Stability, Tip Shapes, Compressibility and Noise for Hovering Model Rotors. NASA CR 2305, Sept. 1973.

53. Tyler, J. M.; and Sofrin, T. G.: Axial Flow Compressor Noise Studies. TRANS SAE, 1961, pp. 309-332.

54. Bramwell, A. R. S.: Aerodynamic Interference of Helicopters. J. Sound and Vibration, vol. 3, no. 3, May 1966.

55. Pegg, R. J.; and Shidler, P. A.: Exploratory Wind-Tunnel Investigation of the Effect of the Main Rotor Wake on Tail Rotor Noise. Helicopter Acoustics Specialists Symp., Hampton, VA, May 1978.

56. Sharland, I. J.: Sources of Noise in Axial Flow-Fans. J. Sound and Vibration, vol. 1, no. 3, pp. 302-322, 1964.

57. Curle, N.: The Influence of Solid Boundaries on Aerodynamic Sound. Proc. of the Royal Society, A-231, 1955.

58. Lowson, M. W.; Whatmore, A. R.; and Whitfield, C. B.: Source Mechanisms for Rotor Noise Radiation. NASA CR 2077, Aug. 1973.

59. Kemp, N. H.; and Sears, W. R.: The Unsteady Forces Due to Viscous Wakes in Turbomachinery. J. Aeronautical Sciences, vol. 22, no. 7, pp. 478-483, July 1955.

60. Brown, David; and Ollerhead, J. B.: Propeller Noise at Low Tip Speeds. AFAPL-TR-71-56. 1971.

61. Bull, M. K.; Wilby, J. F.; and Blackman, D. R.: Wall Pressure Fluctuations in Boundary Layer Flow, and Response of Simple Structures. Southampton Univ. Report AASU 243, July 1963.

62. Clark, David R.: Can Helicopter Rotors be Designed for Low Noise and High Performance? AHS 30th Annual Forum, Washington, May 1971, Preprint No. 803.

63. Yudin, E. Y.: On the Vortex Sound from Rotating Rods. NACA TM 1136, 1947.

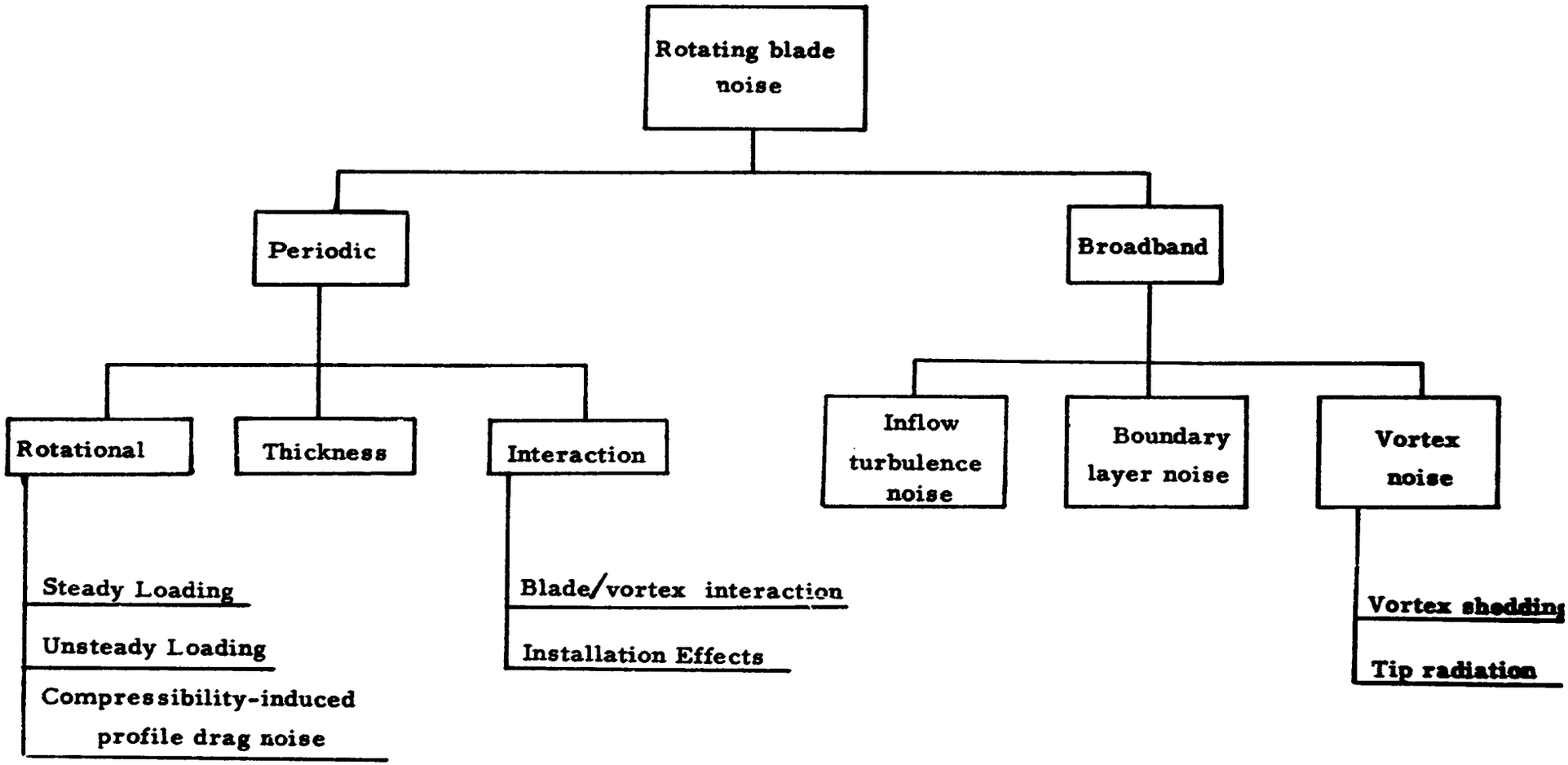

Figure 1. Block diagram of various noise components.

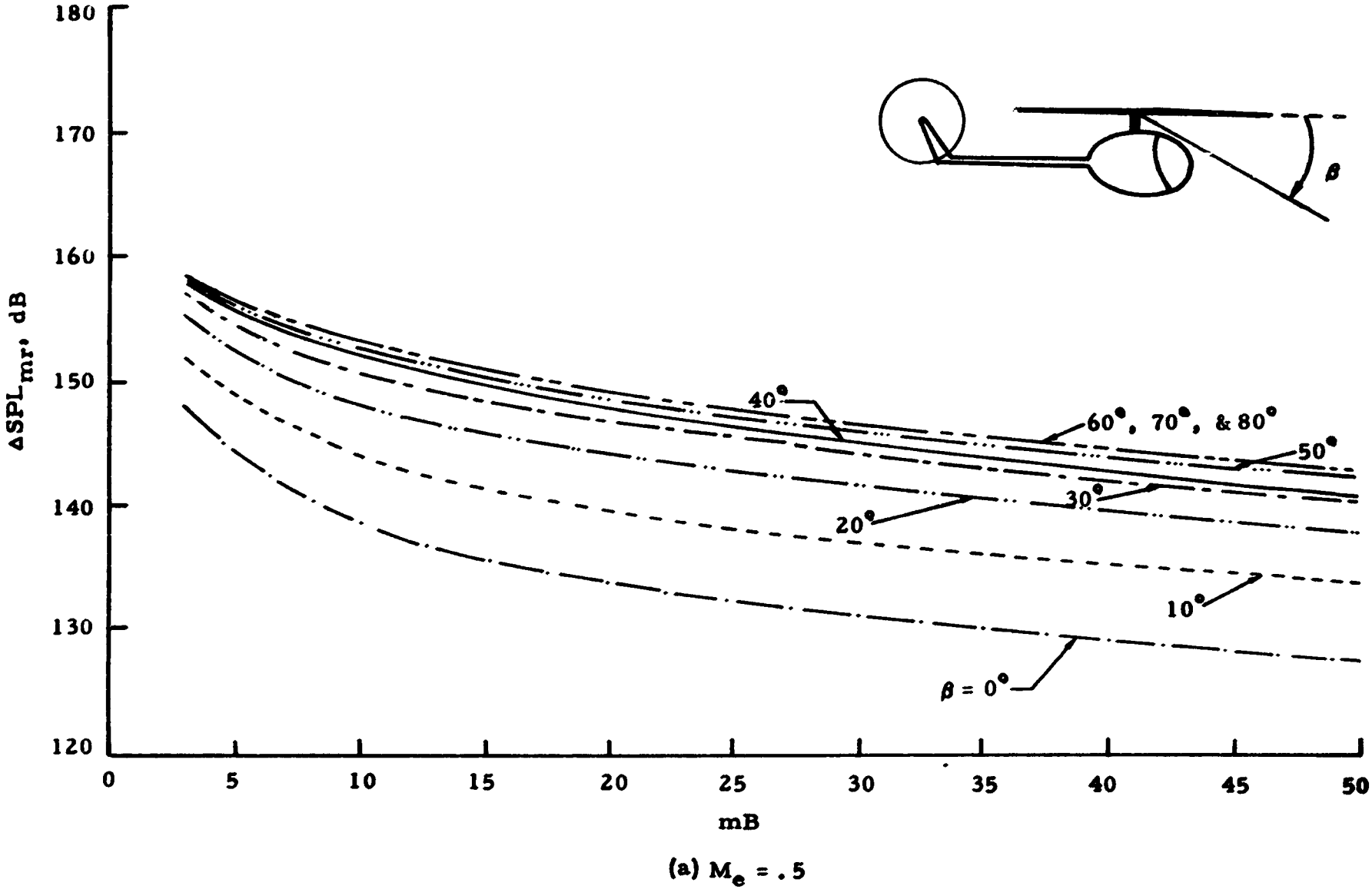

(a) $M_e = .5$

Figure 2. Incremental sound pressure levels for main rotor rotational noise.

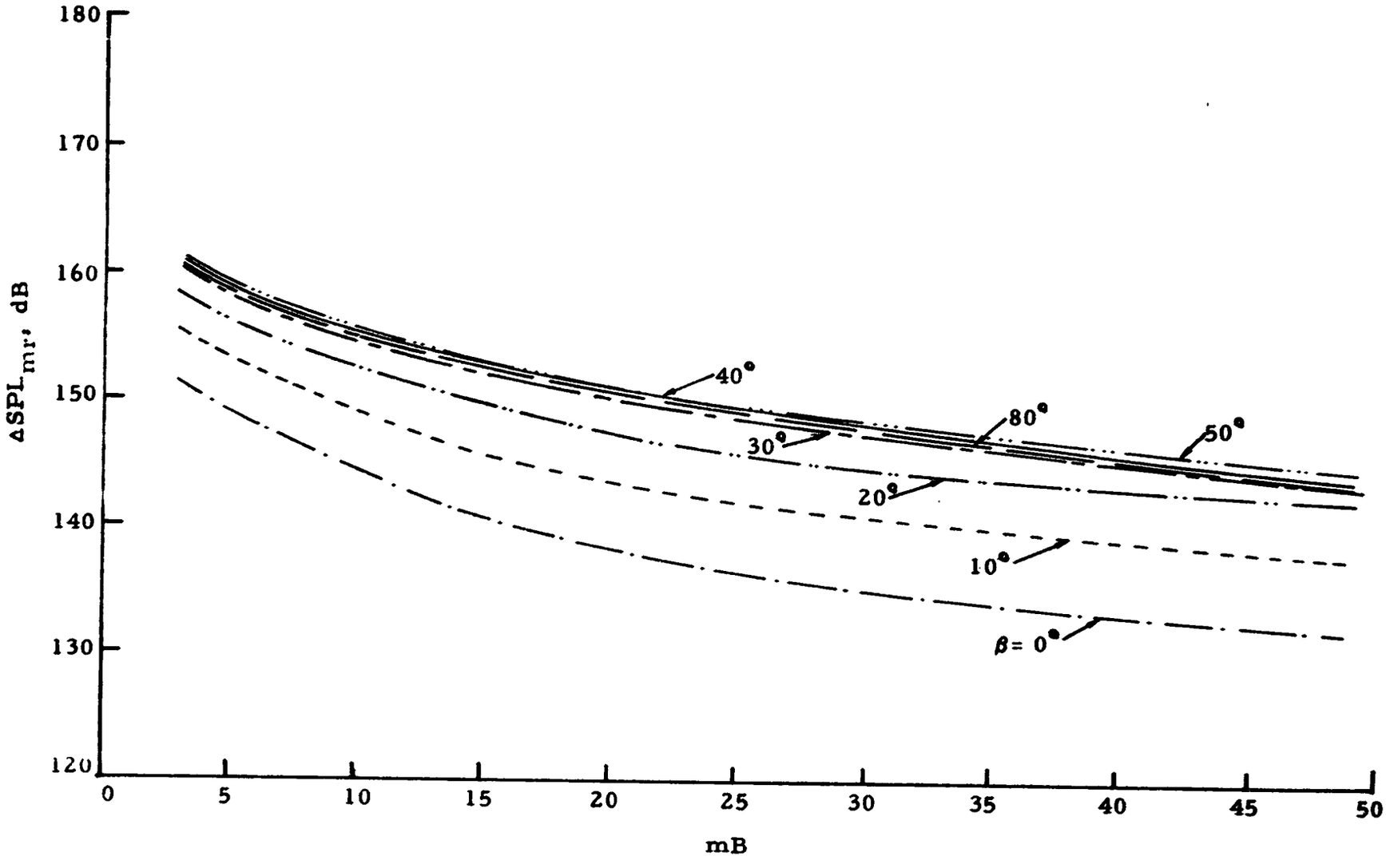

(b) $M_e = .6$

Figure 2. Continued.

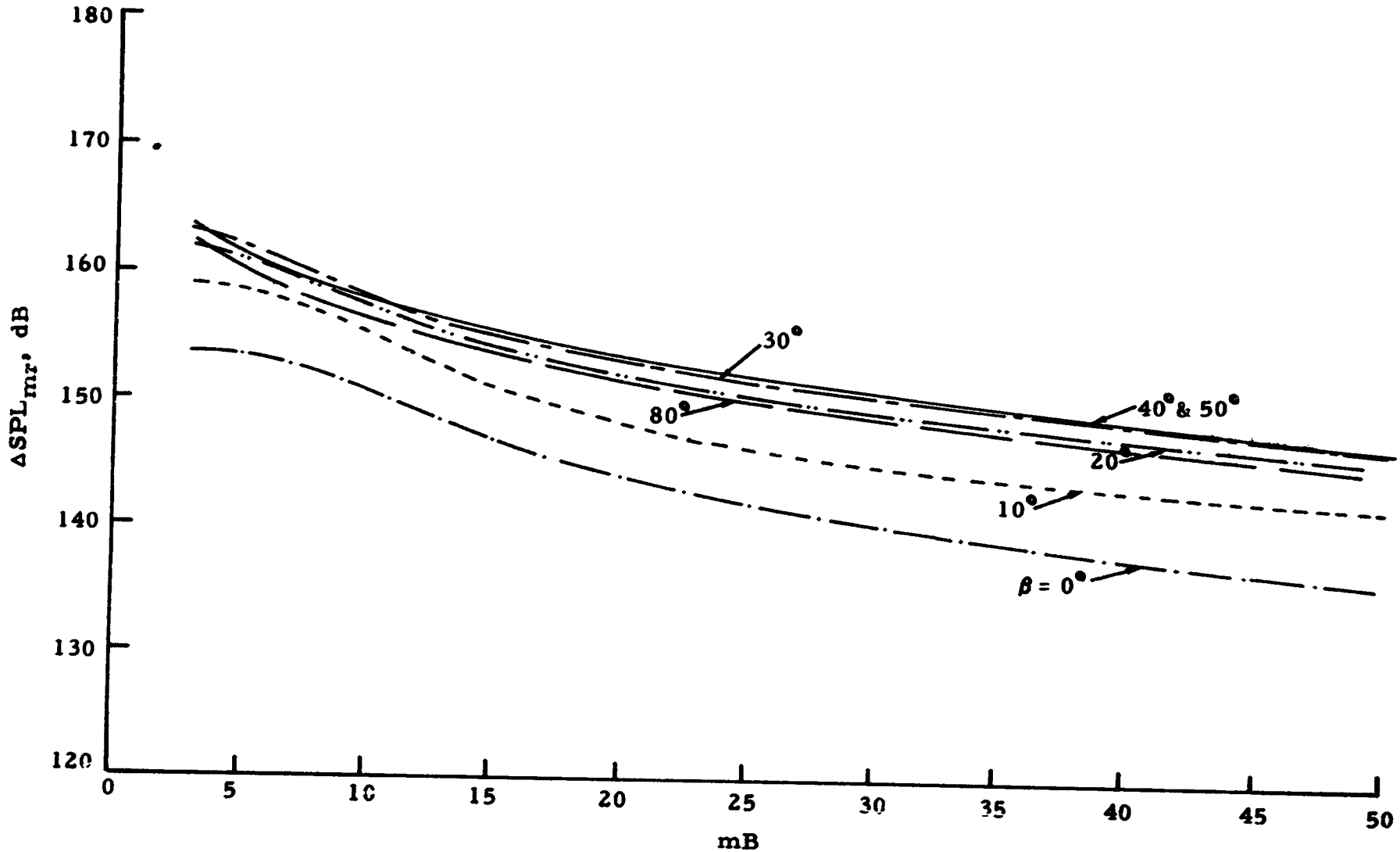

(c) $M_e = .7$

Figure 2. Continued.

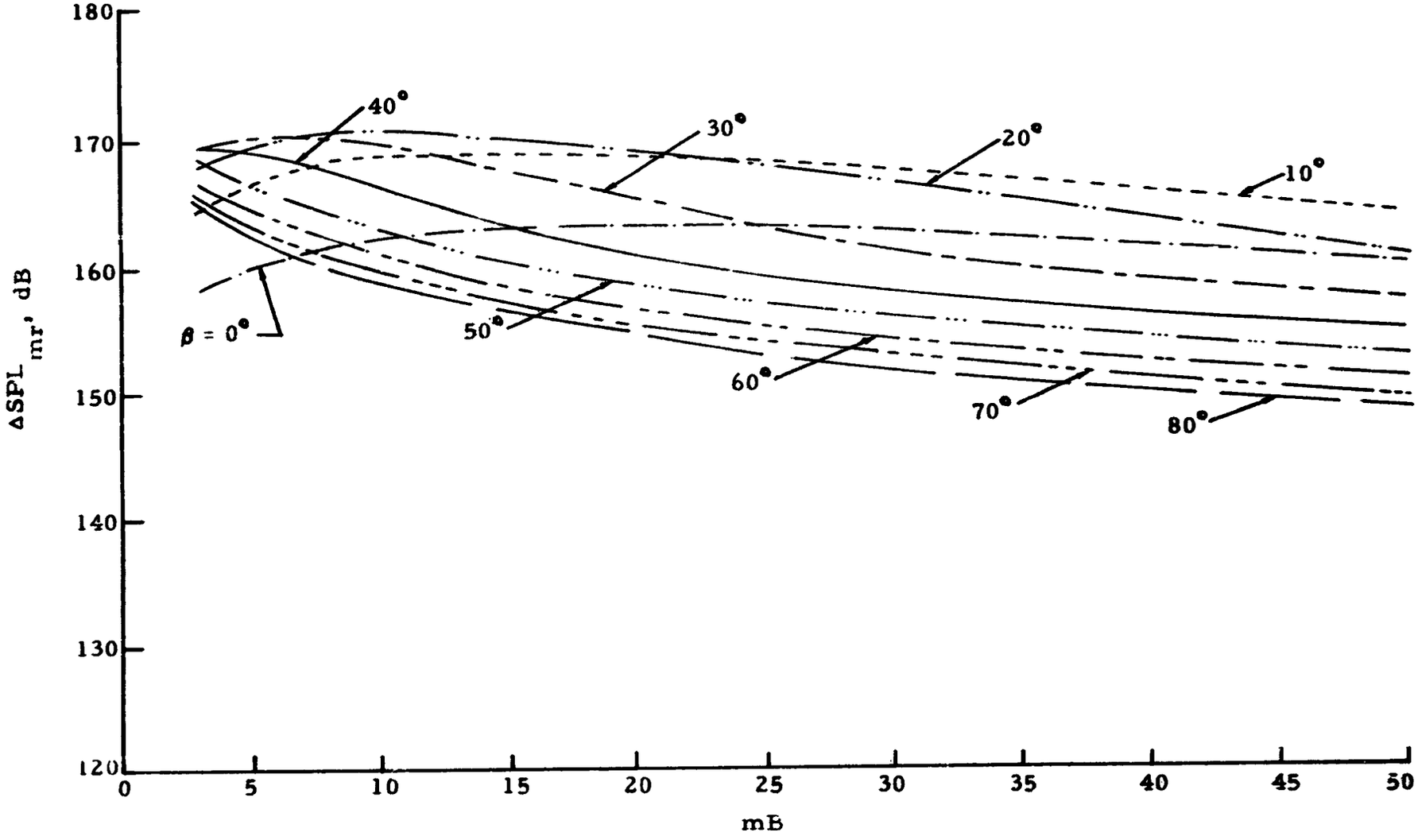

(d) $M_e = .9$

Figure 2. Concluded.

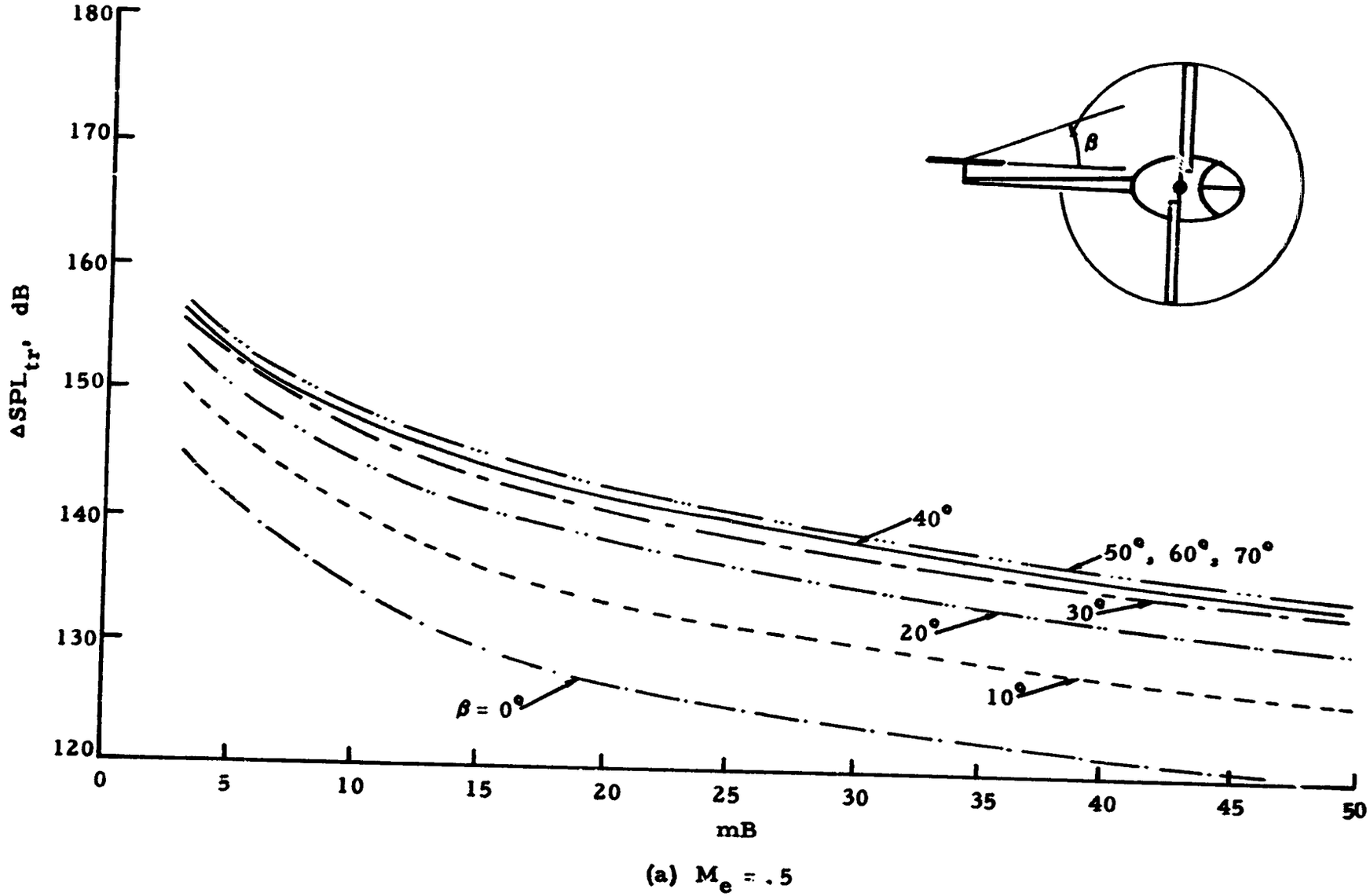

(a) $M_e = .5$

Figure 3. Incremental sound pressure levels for tail rotor rotational noise.

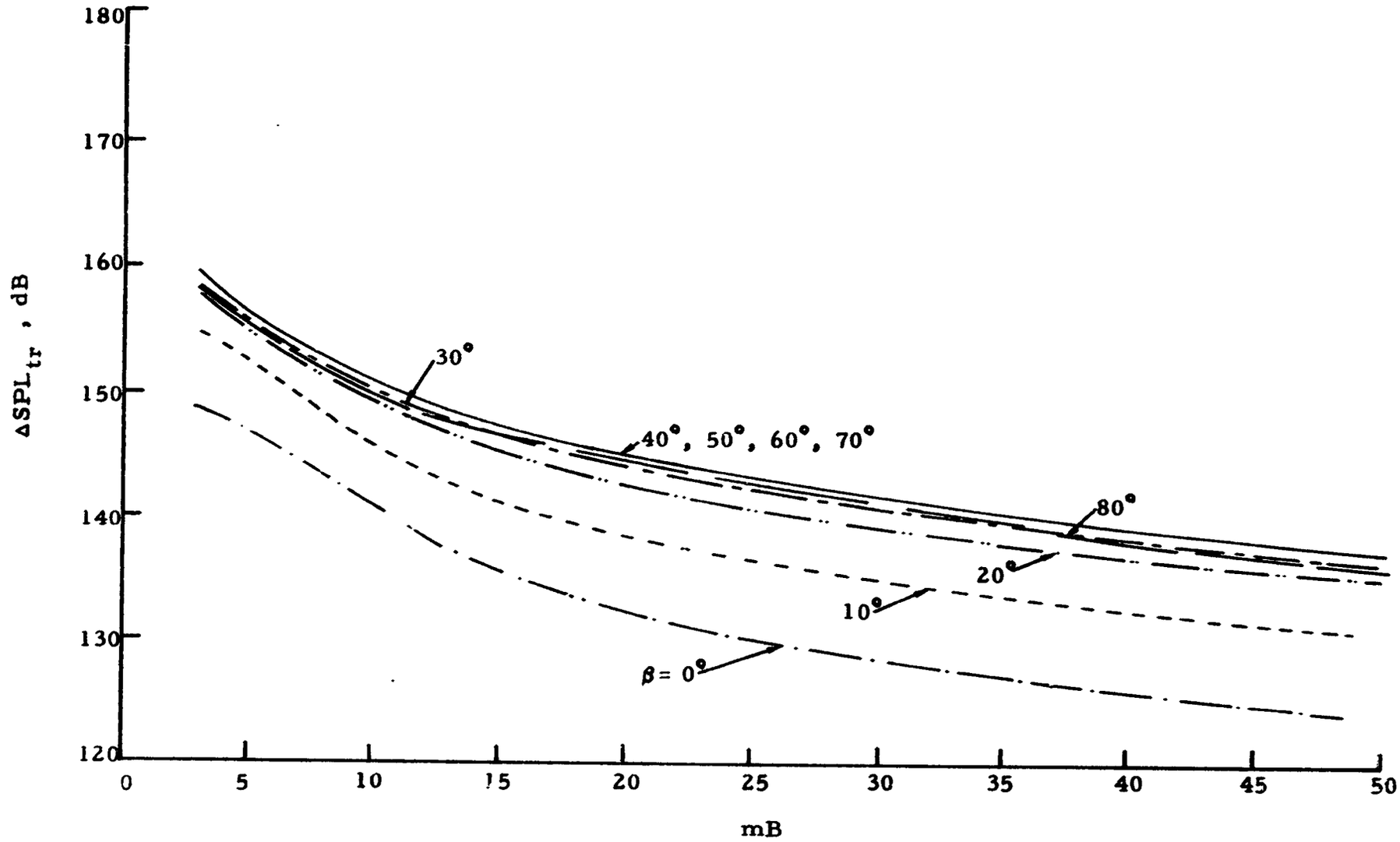

(b) $M_e = .6$

Figure 3. Continued.

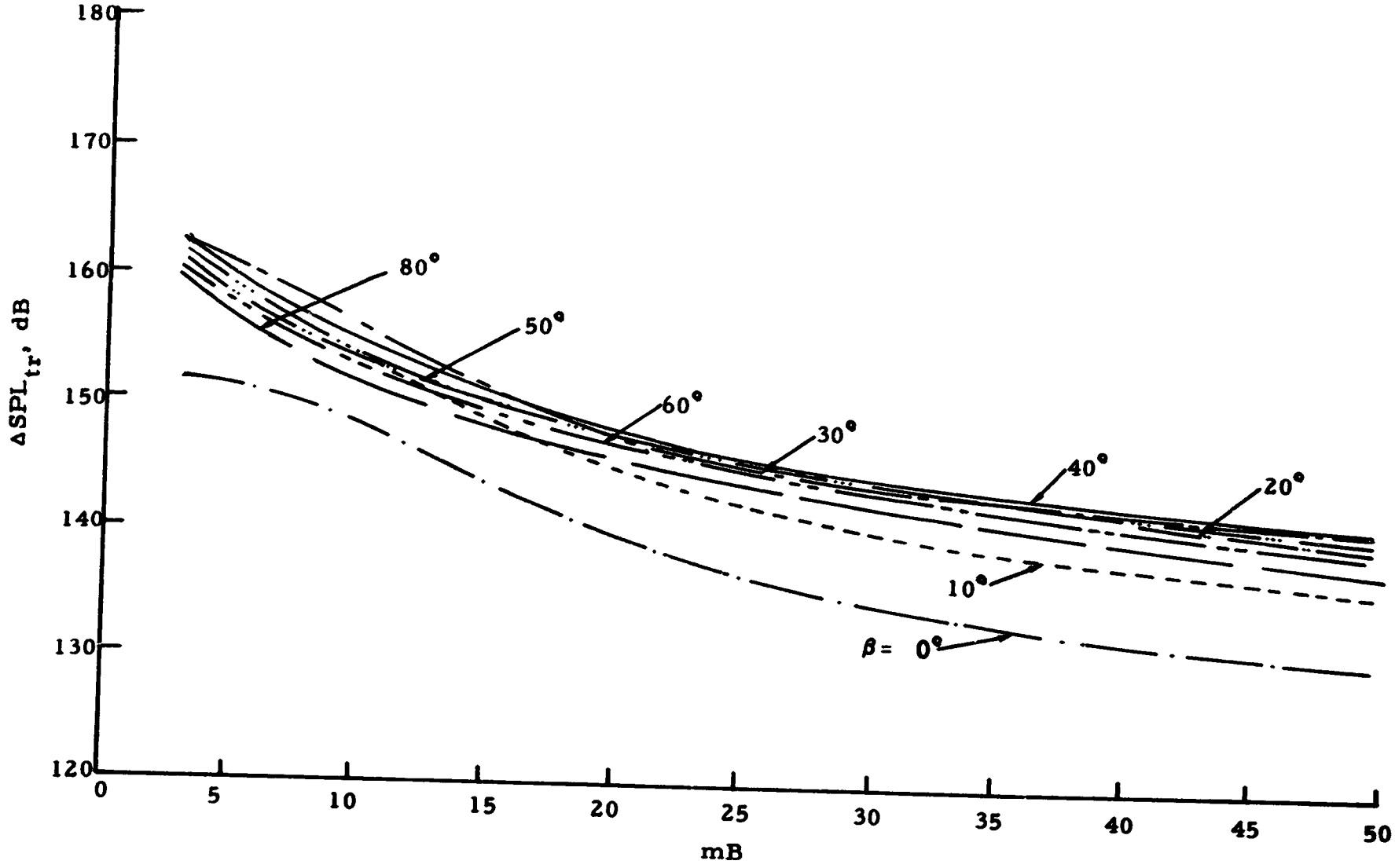

(c) $M_e = .7$

Figure 3. Continued.

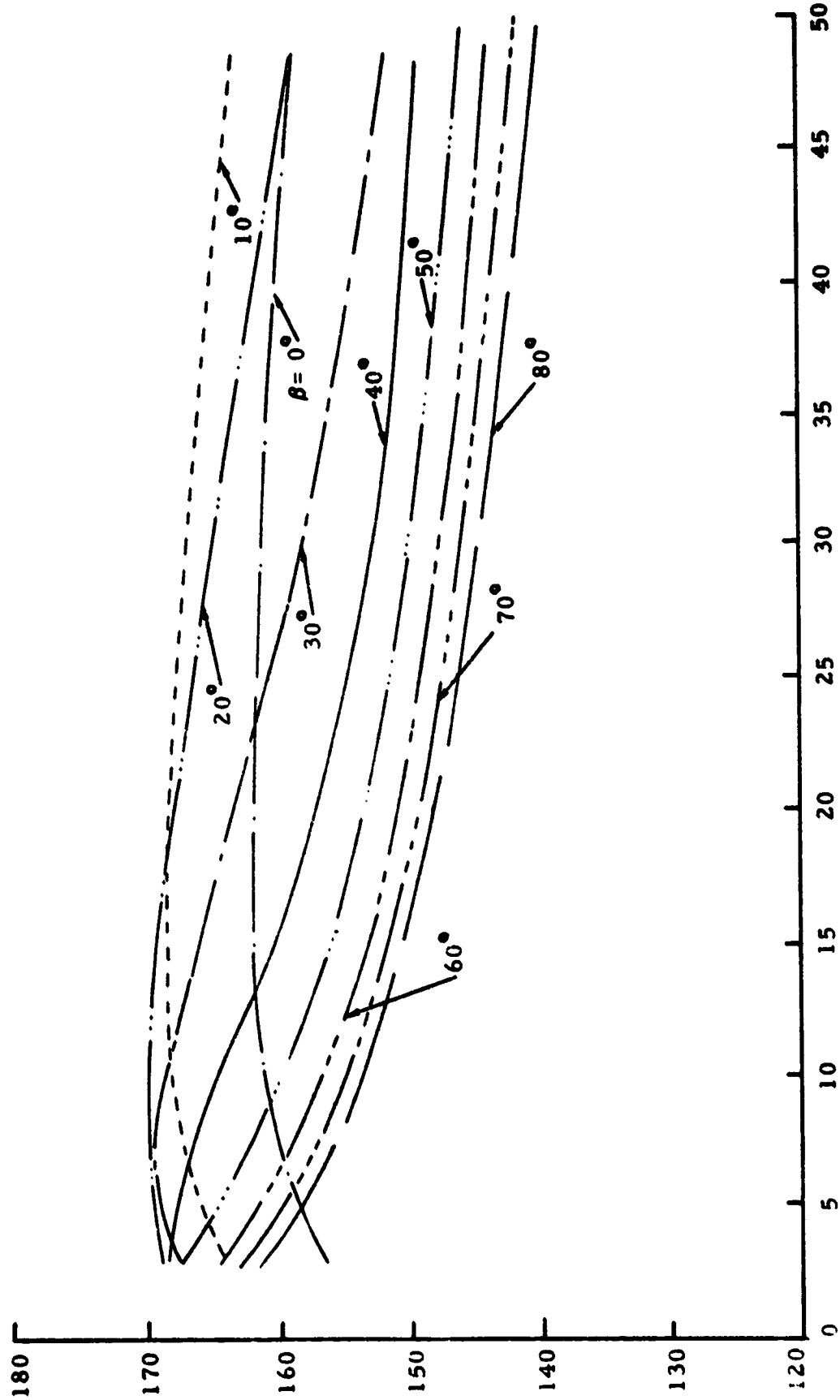

(d) $M_e = .9$

Figure 3. Concluded.

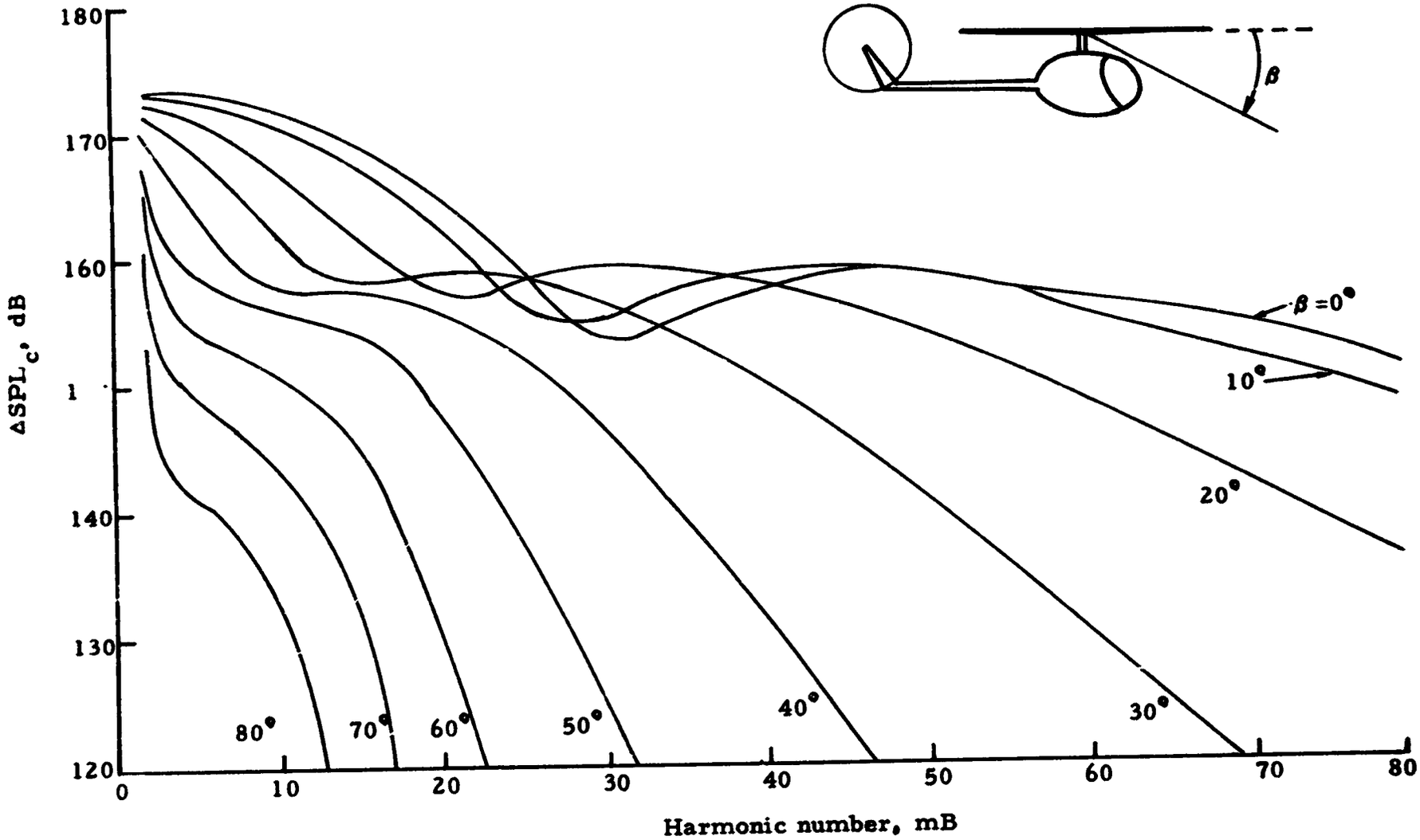

(a) $M_e = .85$

Figure 4. Incremental sound pressure level for the compressibility-induced drag noise.

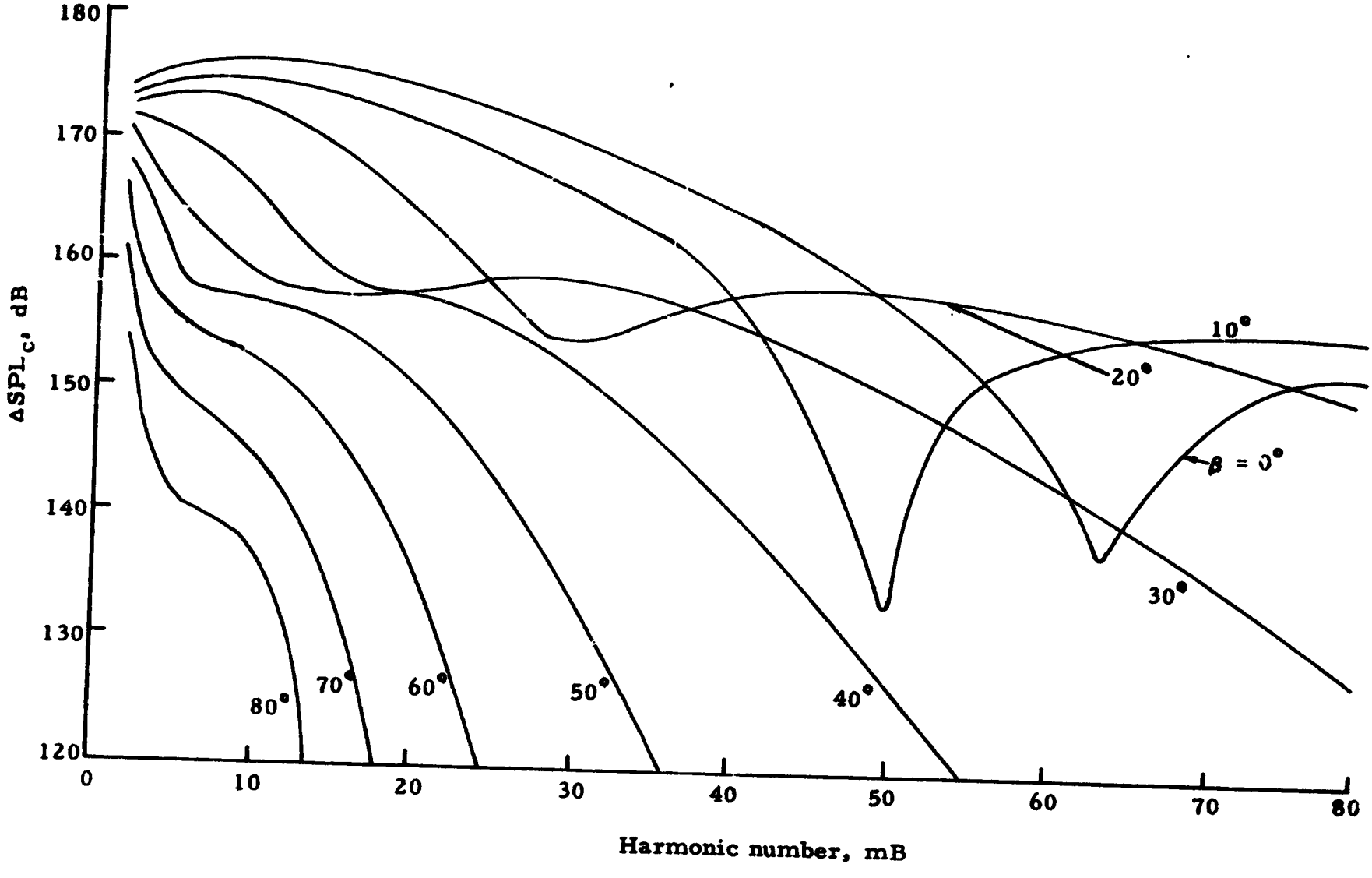

(b) $M_e = .90$

Figure 4. Continued.

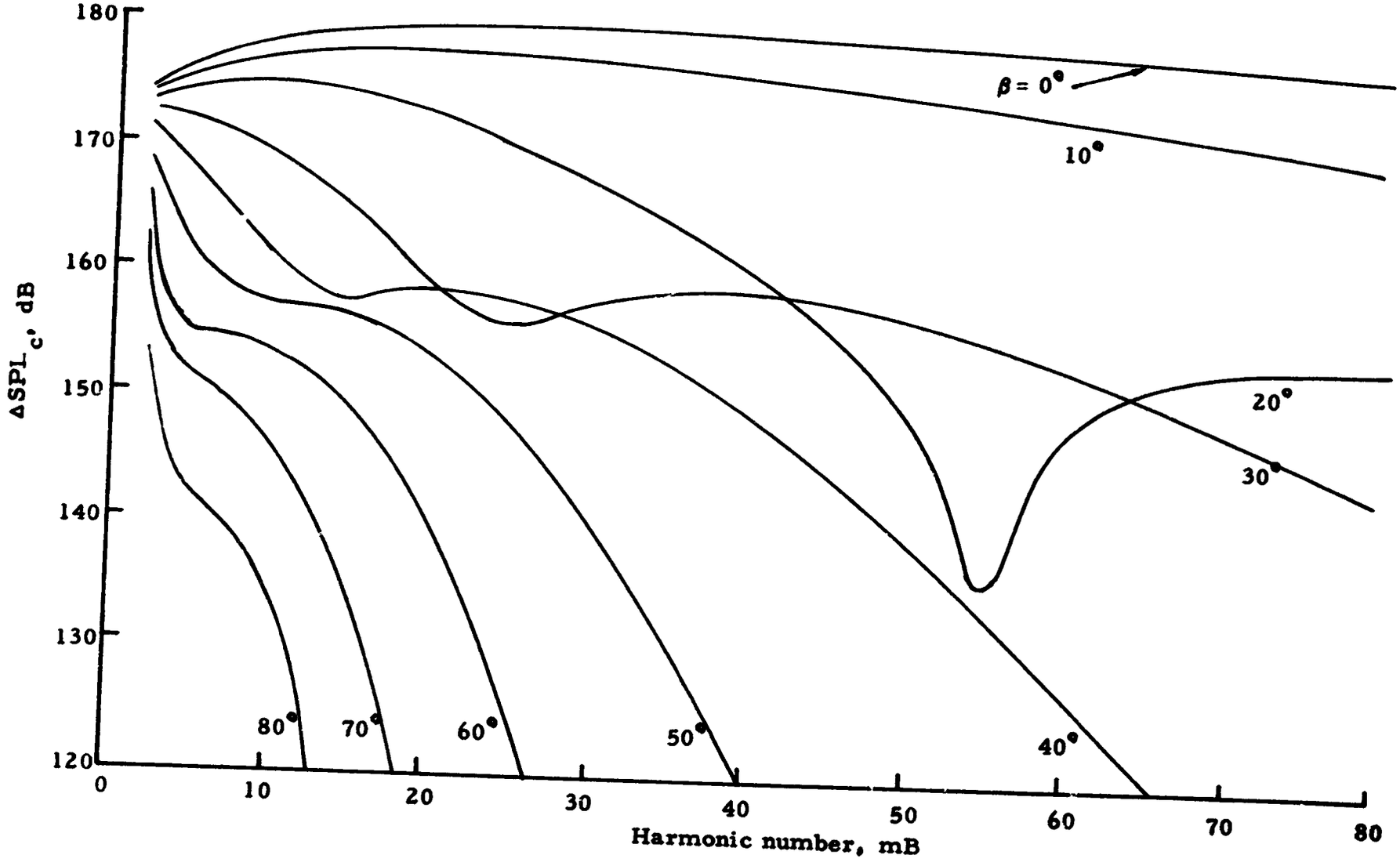

(c) $M_e = .95$

Figure 4. Concluded.

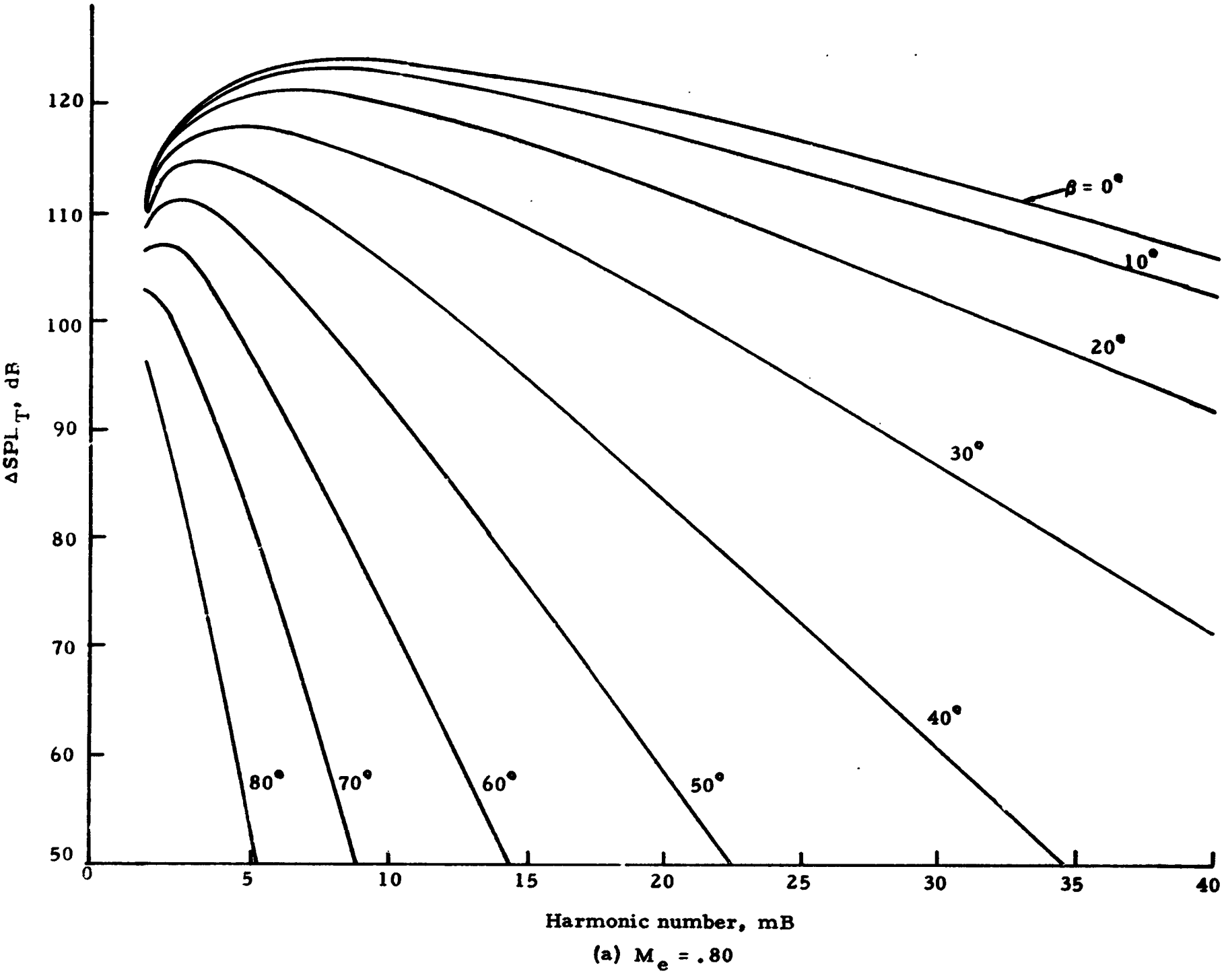

(a) $M_e = .80$

Figure 5. Incremental sound pressure level for thickness noise (k = .03)

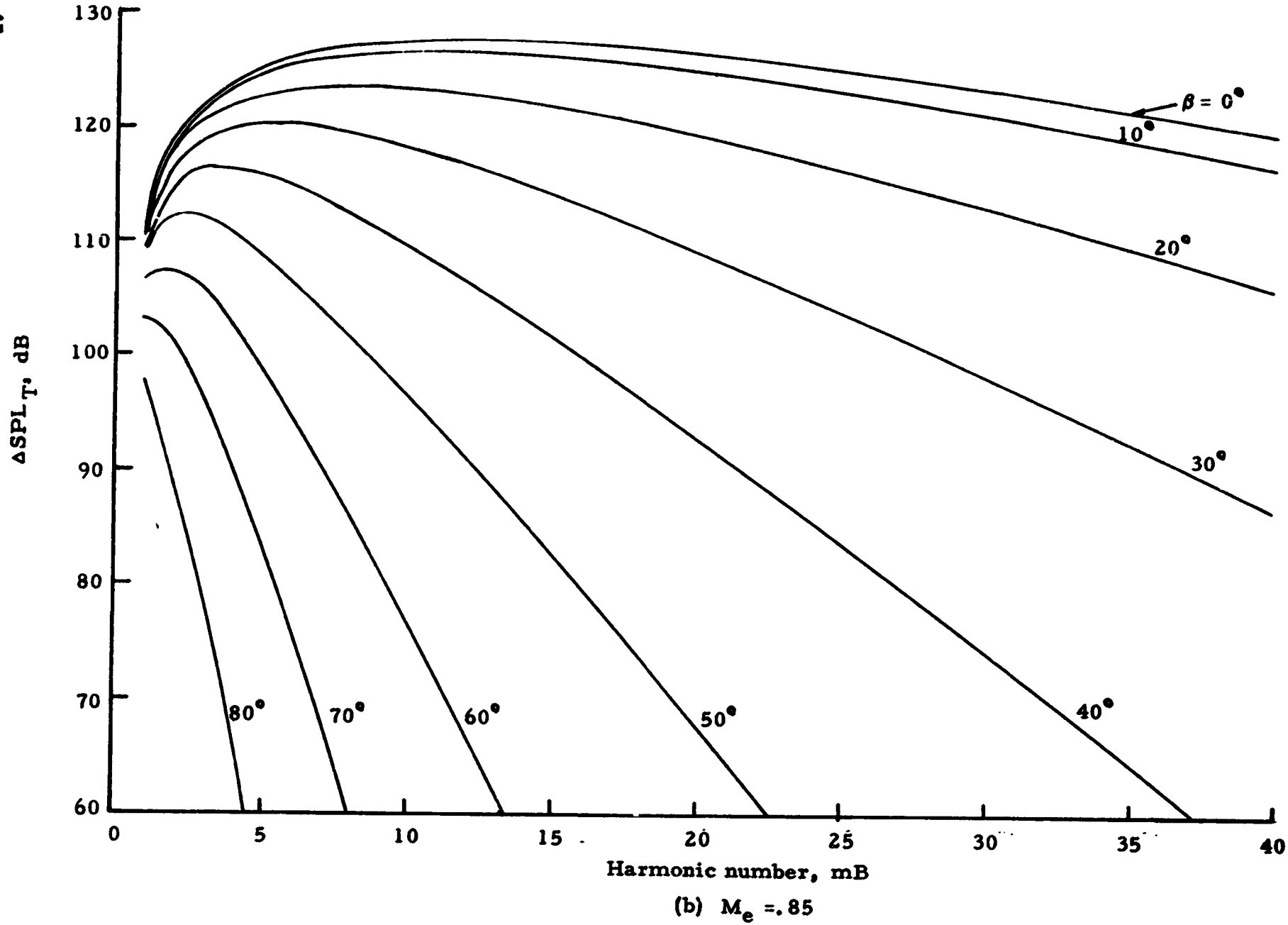

(b) $M_e = .85$

Figure 5. Continued.

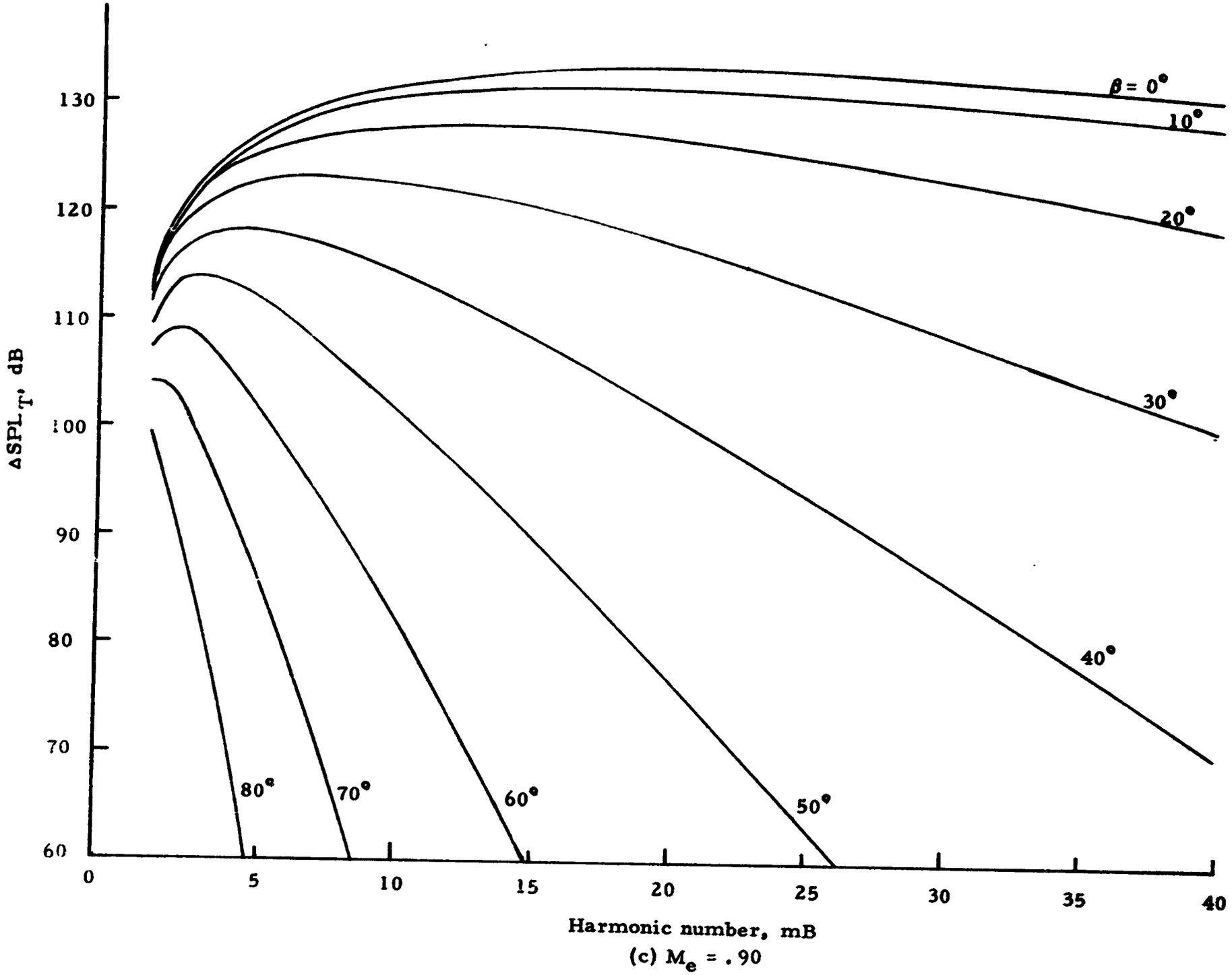

(c) $M_e = .90$

Figure 5. Continued.

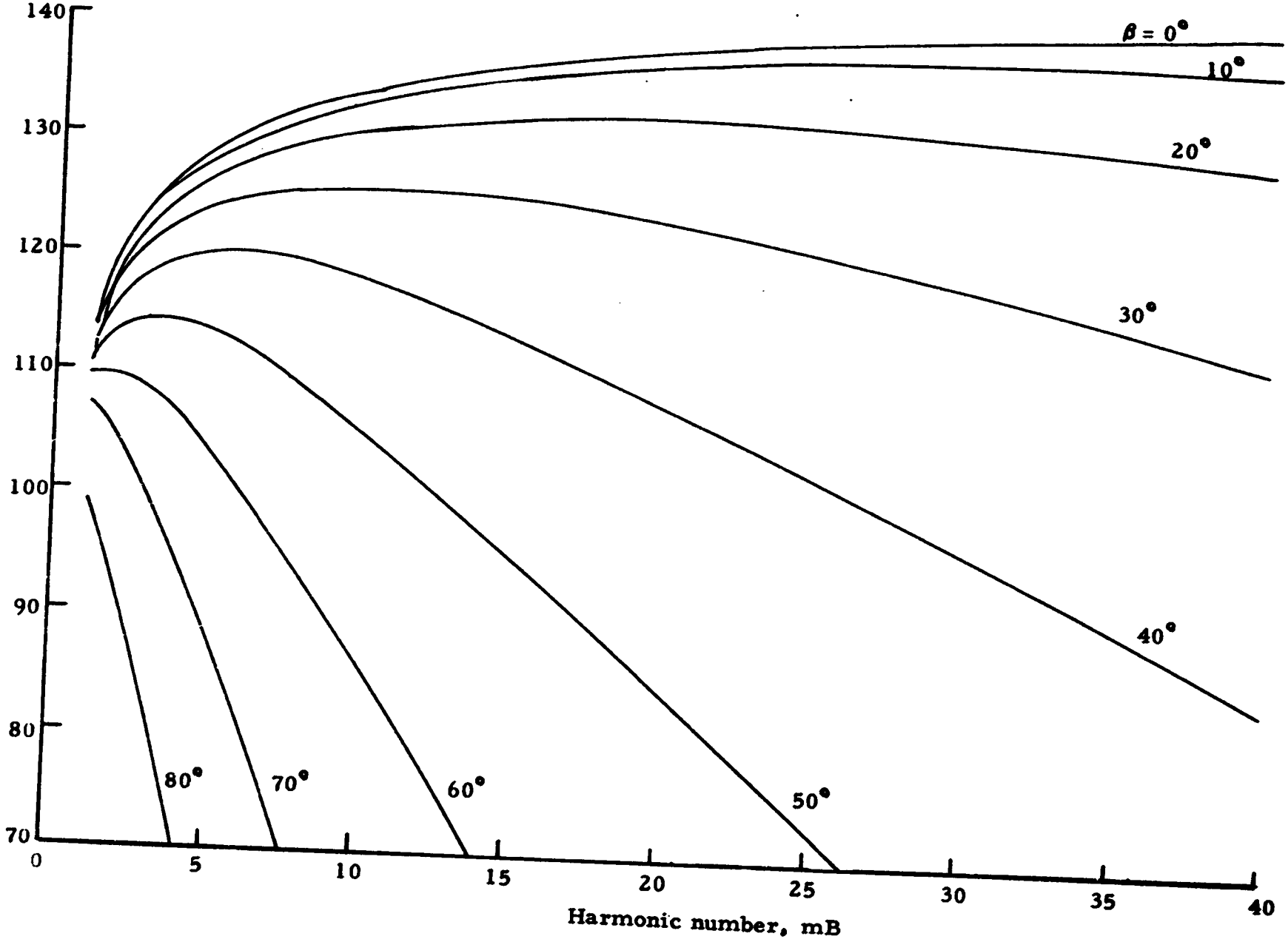

(d) $M_e = .95$

Figure 5. Concluded.

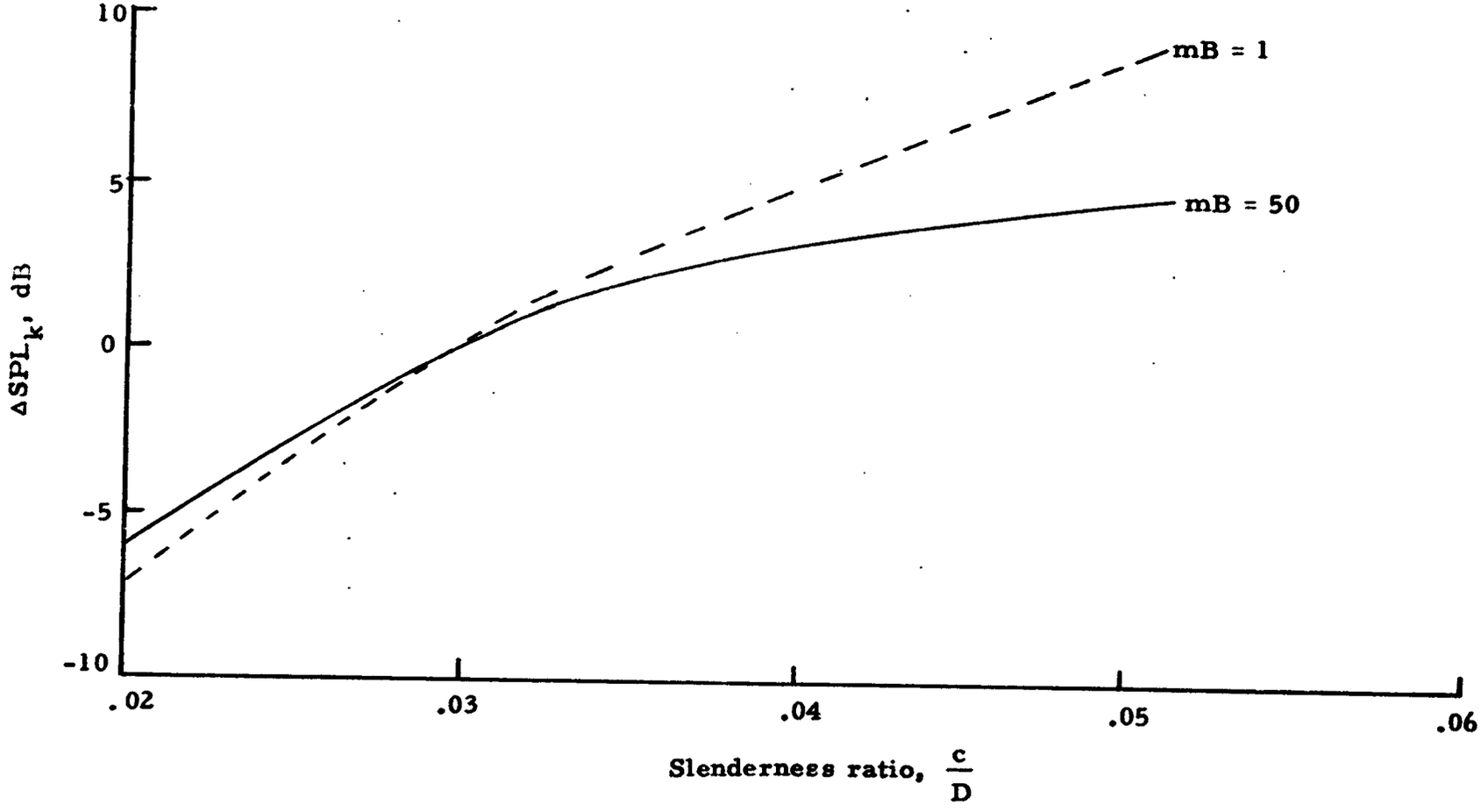

Figure 6. Thickness noise correction curves for rotors having various slenderness ratios.

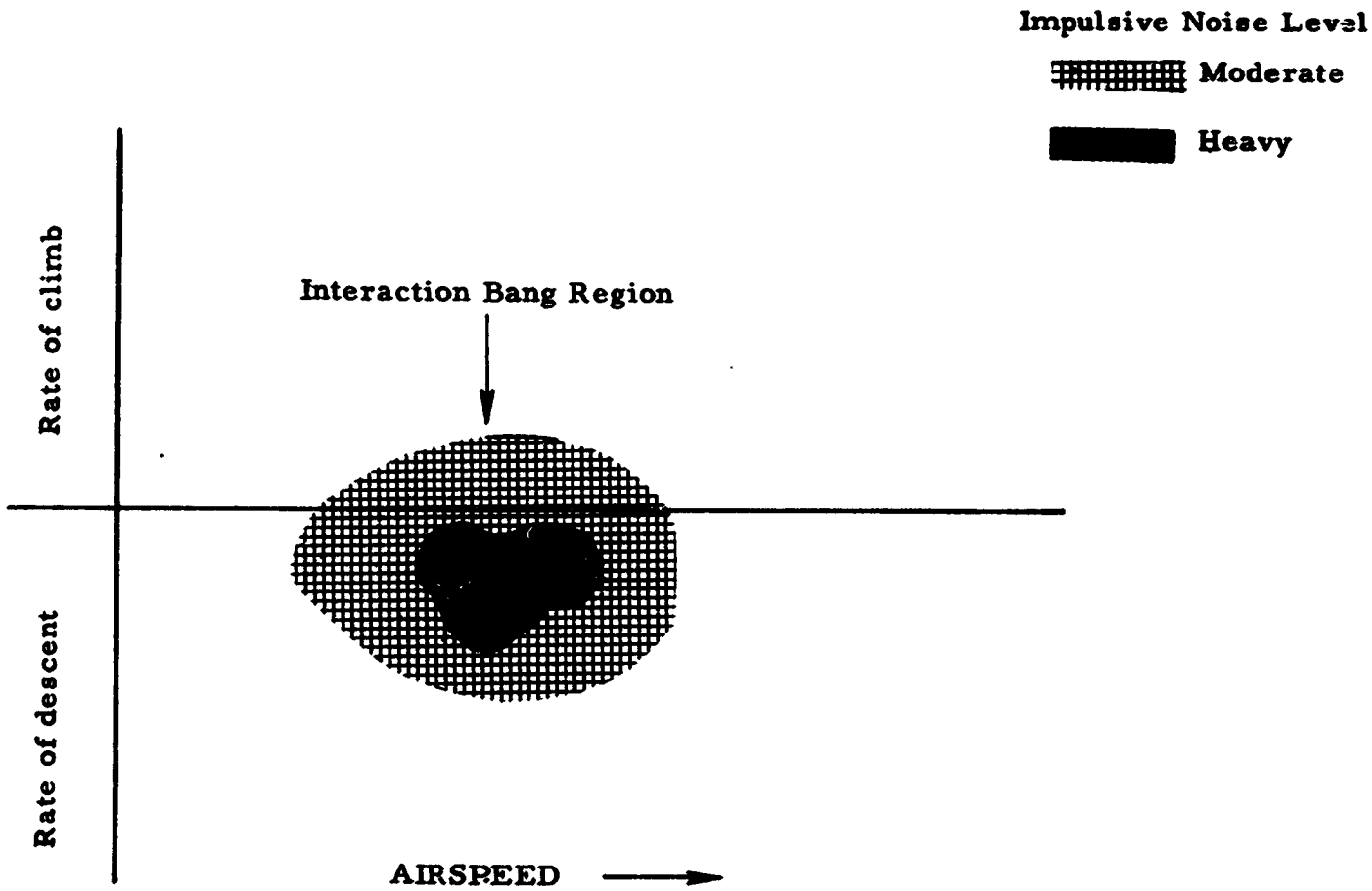

Figure 7. Example of flight region where blade/vortex impulsive rotor noise may be expected.

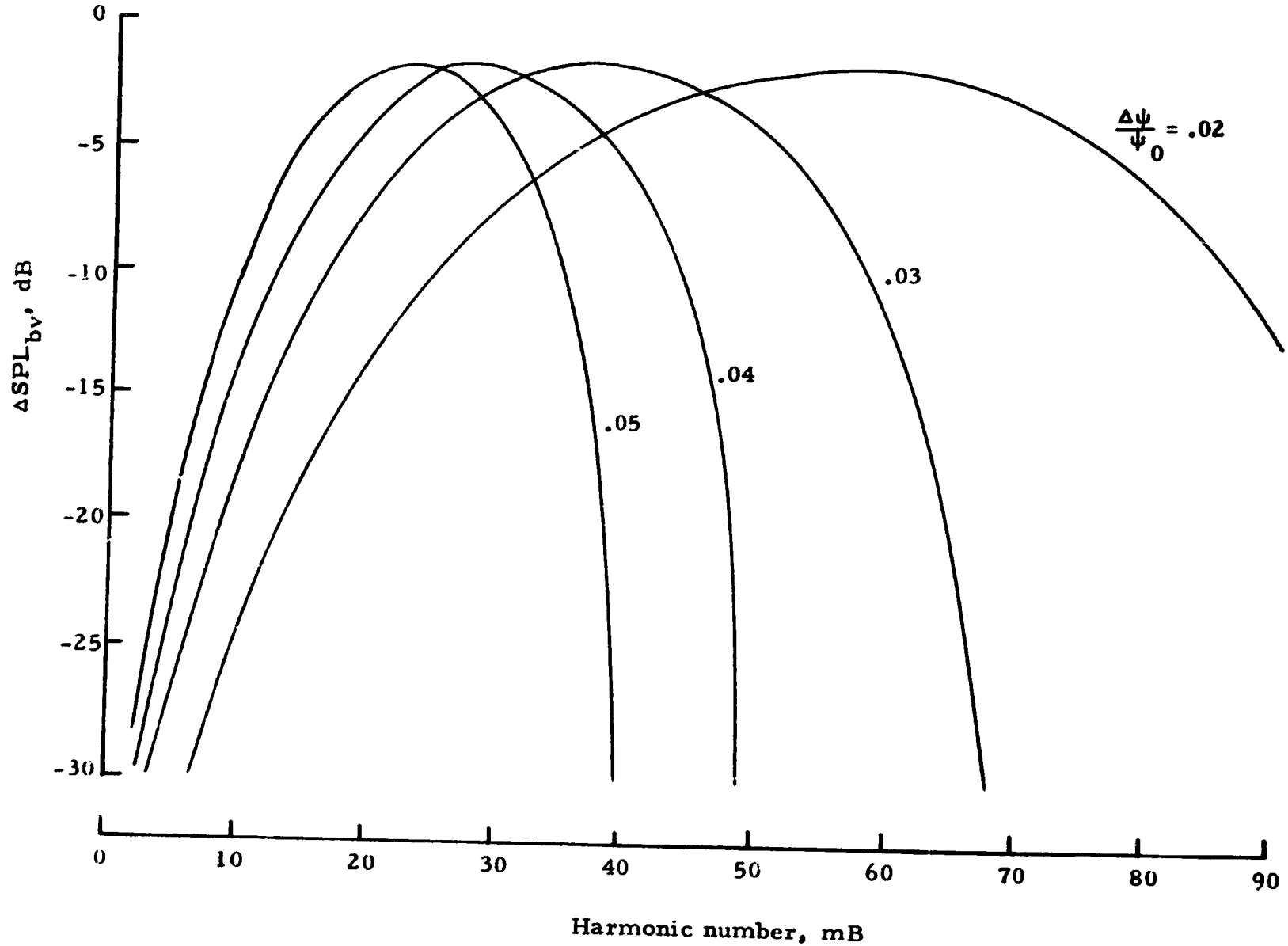

Figure 8. Incremental sound pressure level for blade-vortex interaction noise.

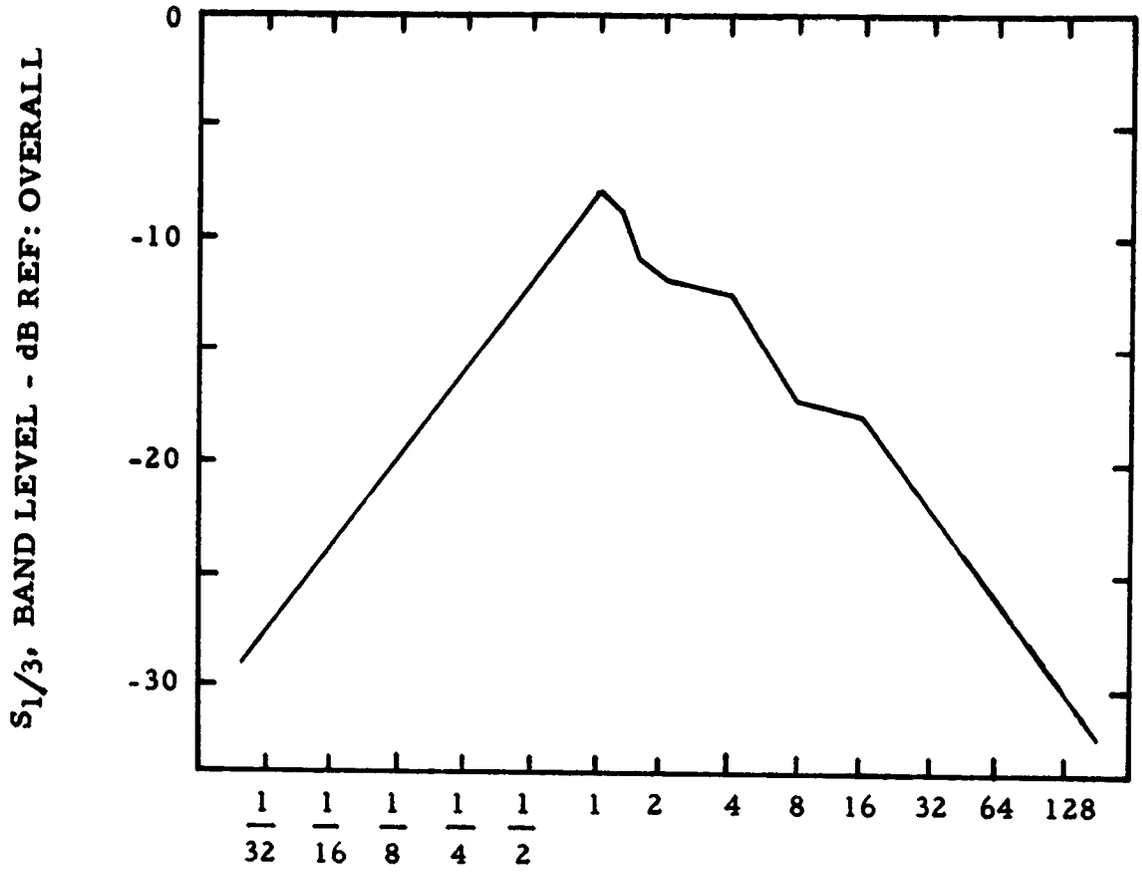

BAND CENTER FREQUENCY, BAND LEVEL

1/32= -29.0	2 = -11.5
1/16 = -24.5	4 = -12.1
1/8 = -19.5	8 = -16.5
1/4 = -15.3	16 = -17.0
1/2 - -11.7	32 = -21.8
1 = -7.5	64 = -26.4
	128 = -30.0

Figure 9. Normalized rotor broadband noise empirically determined spectrum shape.

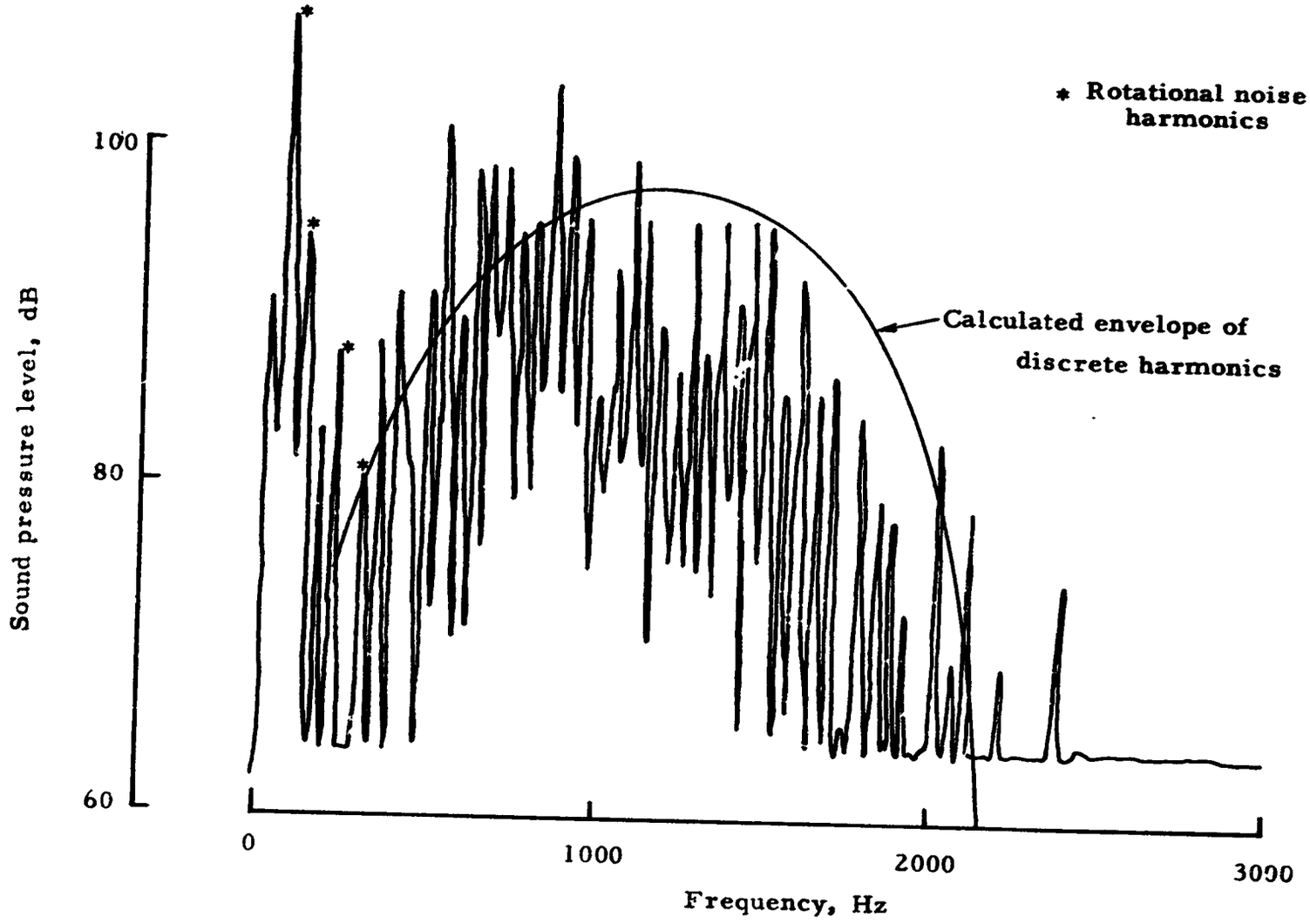

Figure 10. Comparison of measured and calculated acoustic spectra for a 2.1m diameter wind tunnel model in a descent flight condition.

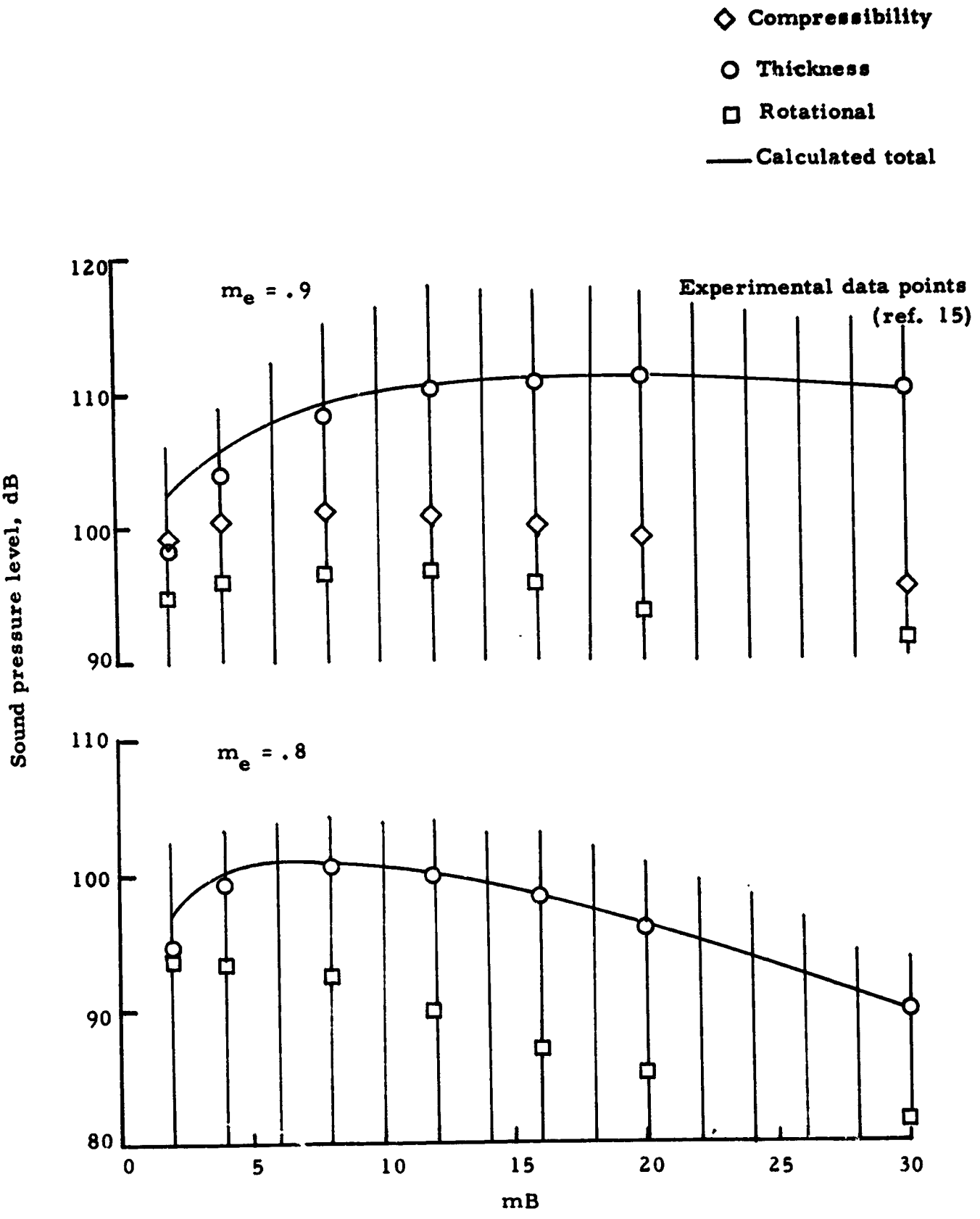

Figure 11. Comparison of calculated and experimental inplane acoustic data for a lifting, hovering rotor.

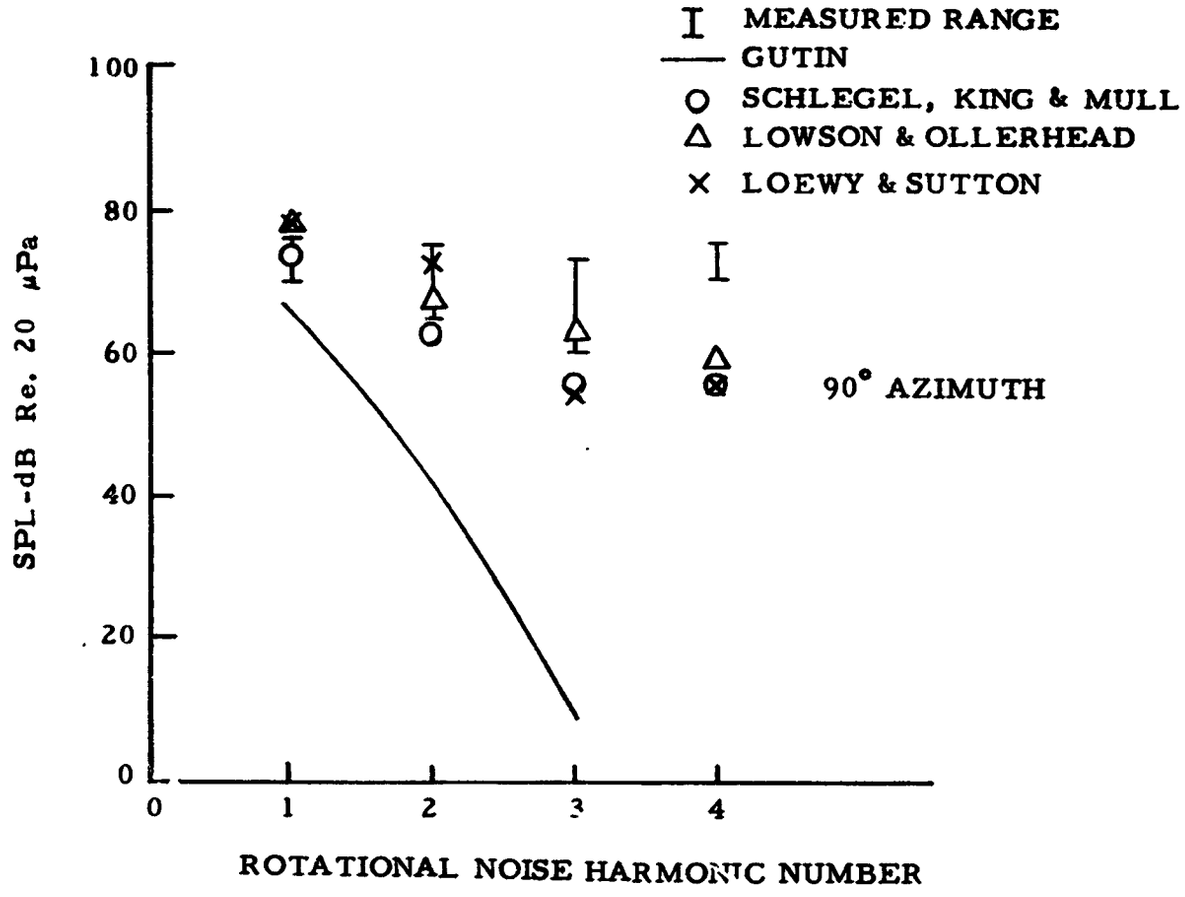

Figure 12. Comparison of experimental data (ref. 11) and Gutin theory based on steady loads.

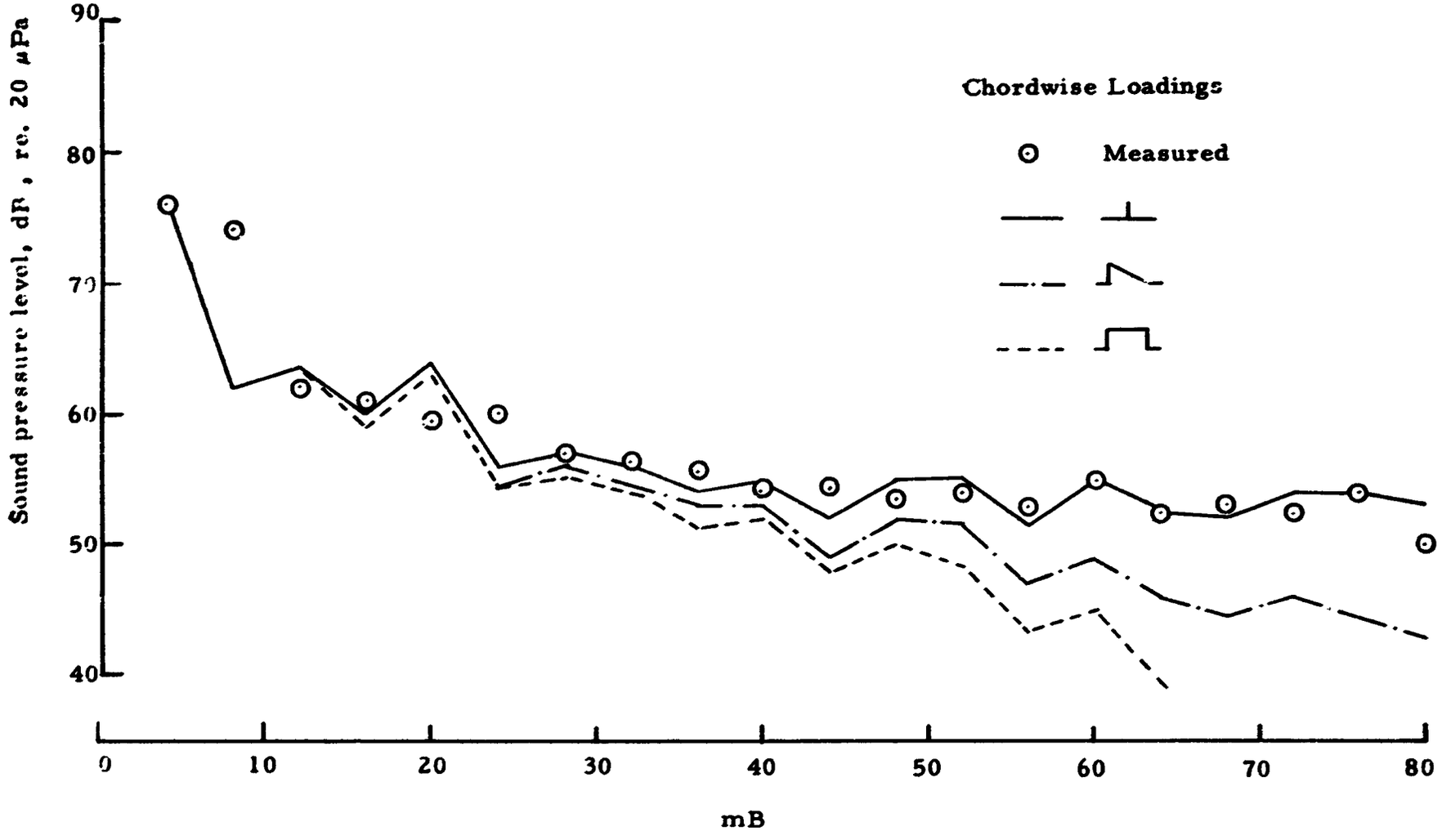

Figure 13. A comparison of a typical measured acoustic spectrum and calculated spectra based on several chordwise loading distributions (ref. 23).

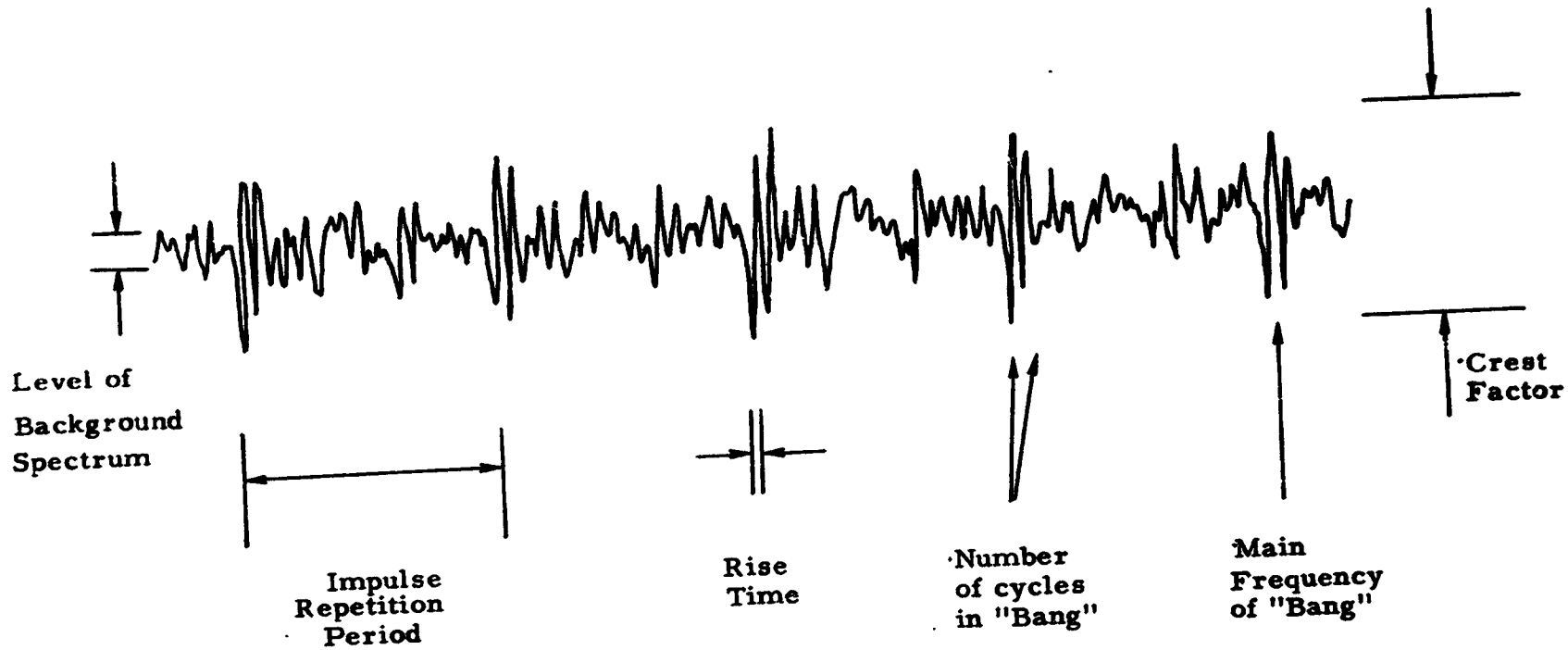

Figure 14. Characteristics of a helicopter blade slap impulsive noise signature.

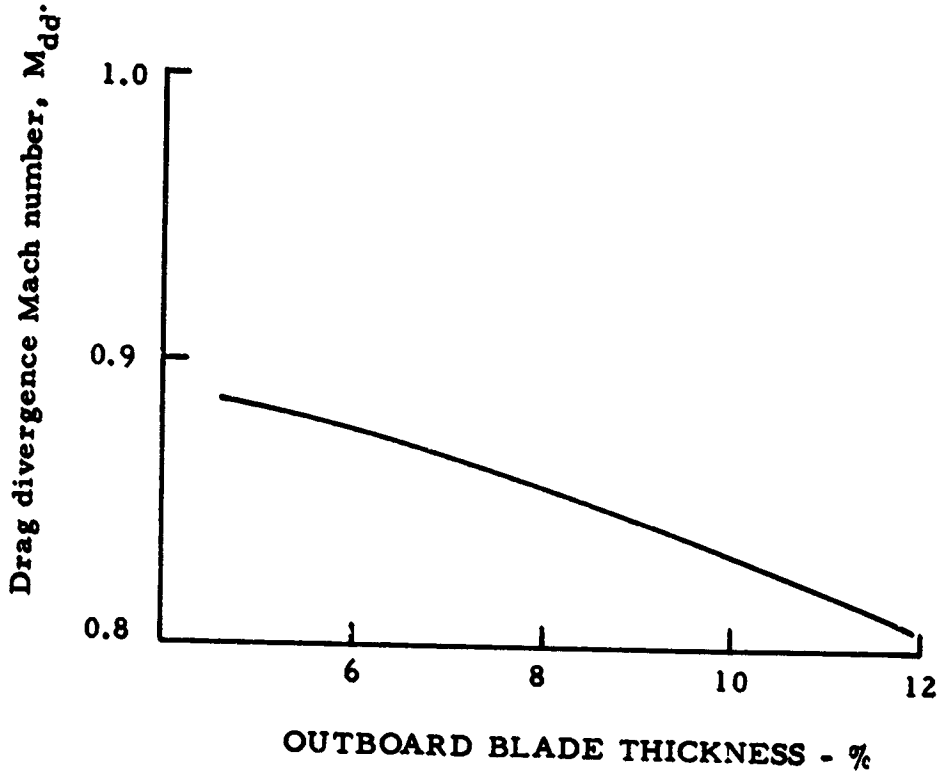

Figure 15. Drag divergence Mach number as a function of tip thickness for typical airfoils used in helicopter rotors.

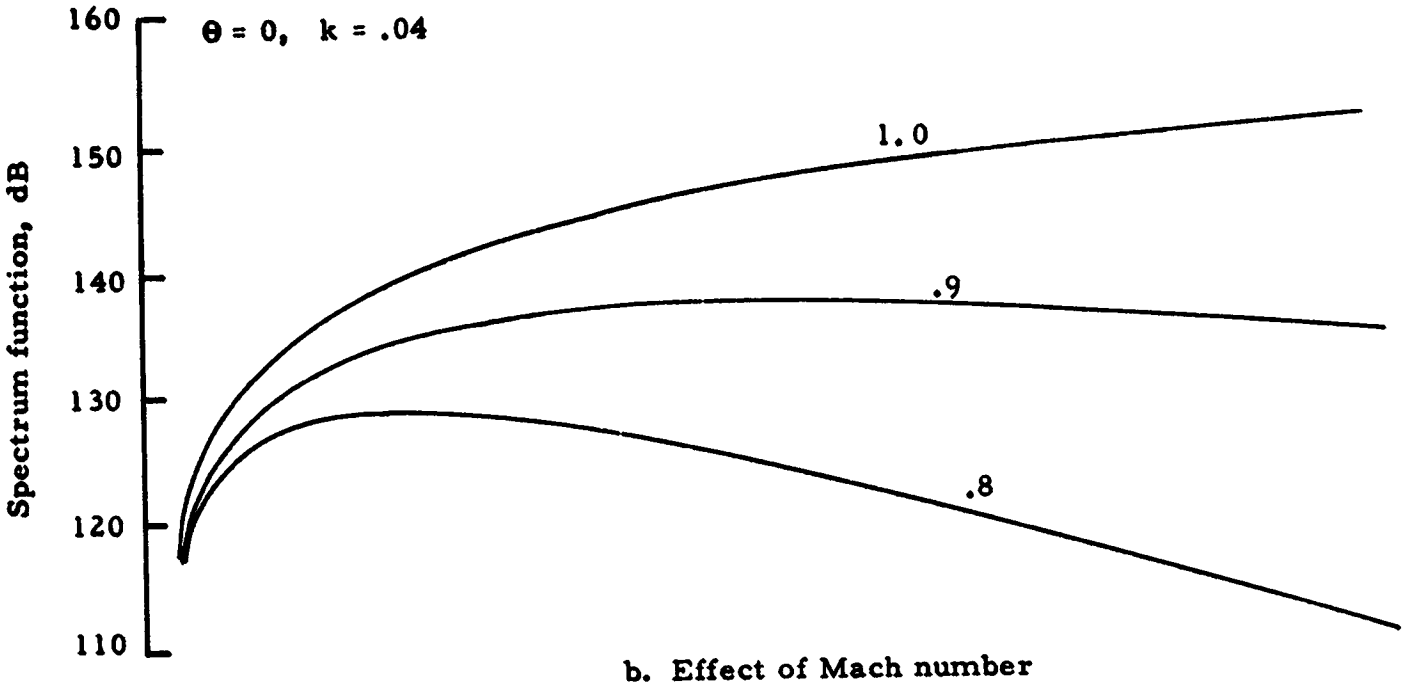

b. Effect of Mach number

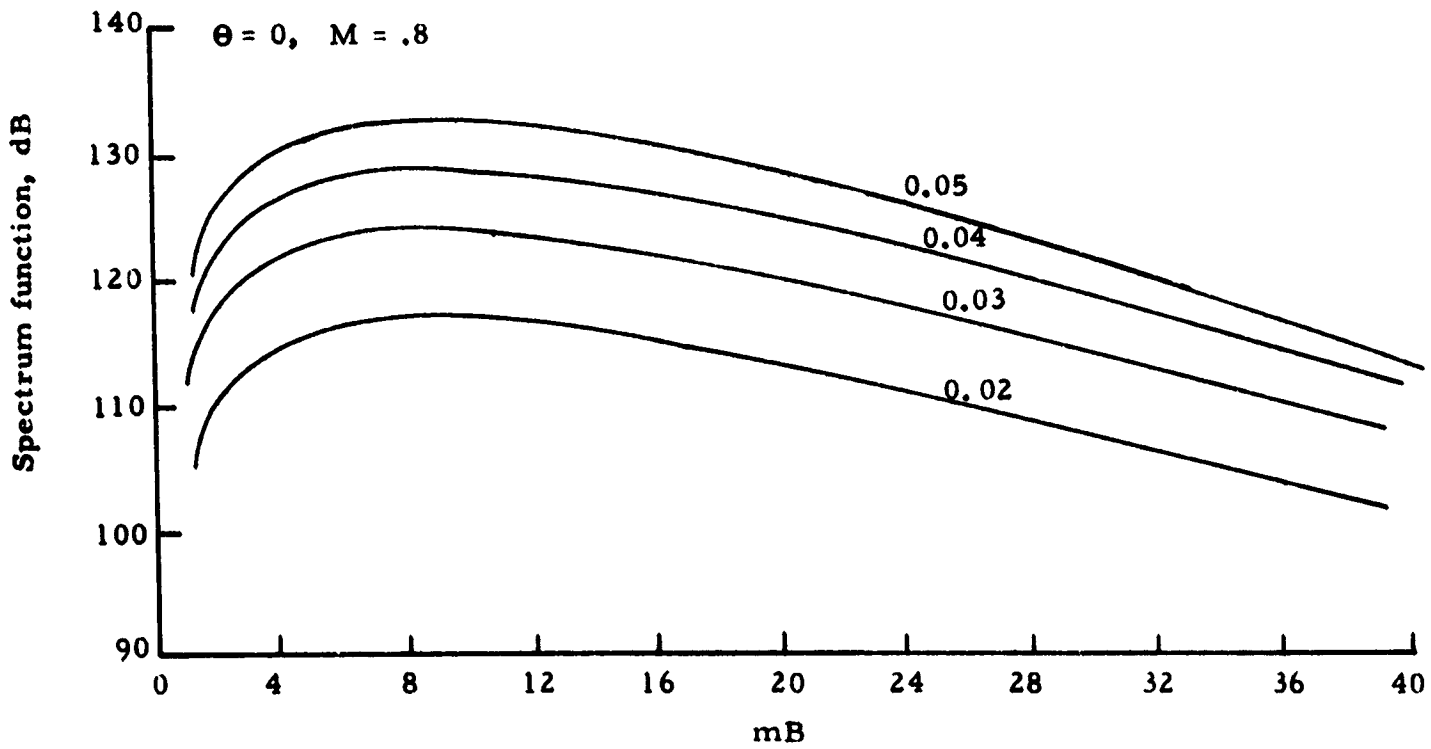

a. Effect of blade slenderness

Figure 16. Thickness noise acoustic spectra shape as a function of Mach number and blade slenderness.

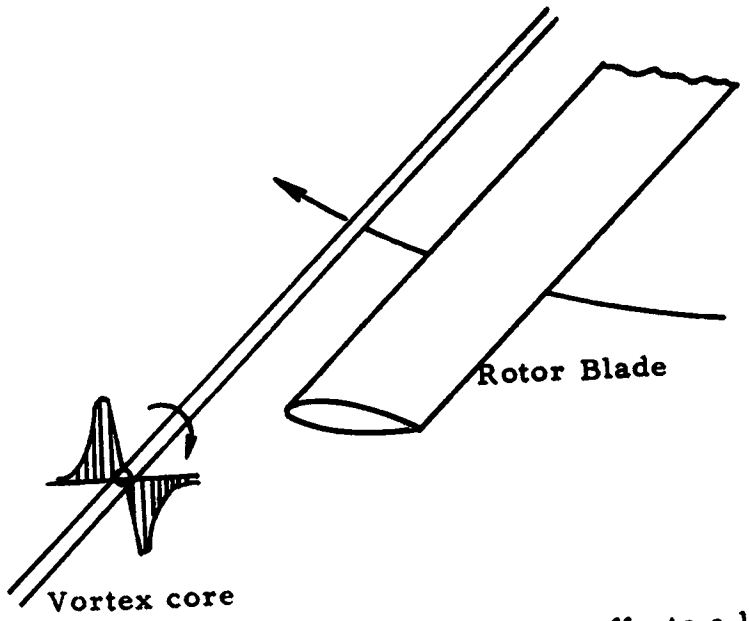

b. Parallel blade/vortex interaction: affects a large portion of the lifting surface for a relatively short period of time.

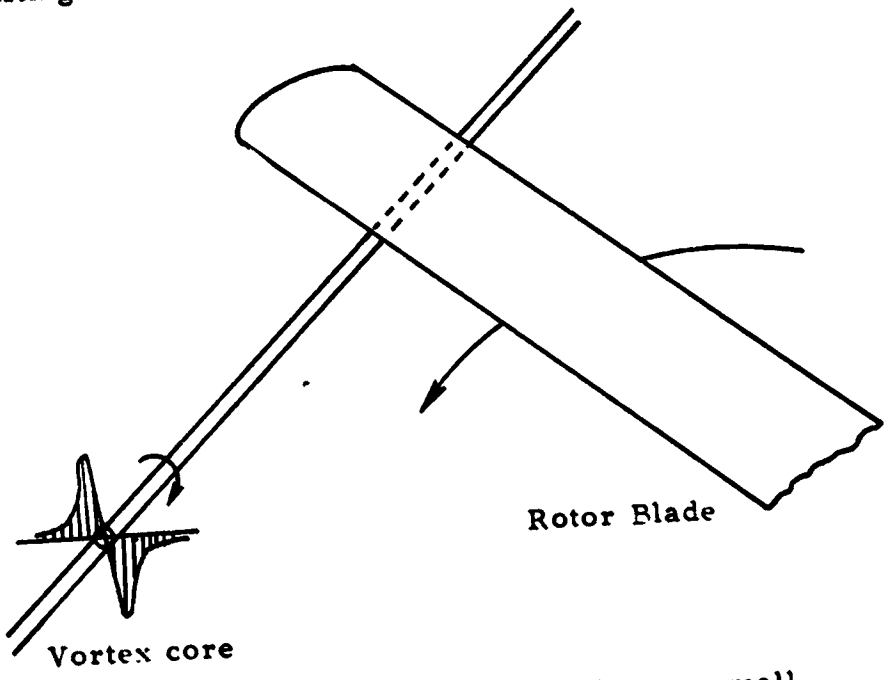

a. Perpendicular blade/vortex interaction: affects a small portion of the lifting surface for a relatively long period of time.

Figure 17. Schematic of blade/vortex interactions.

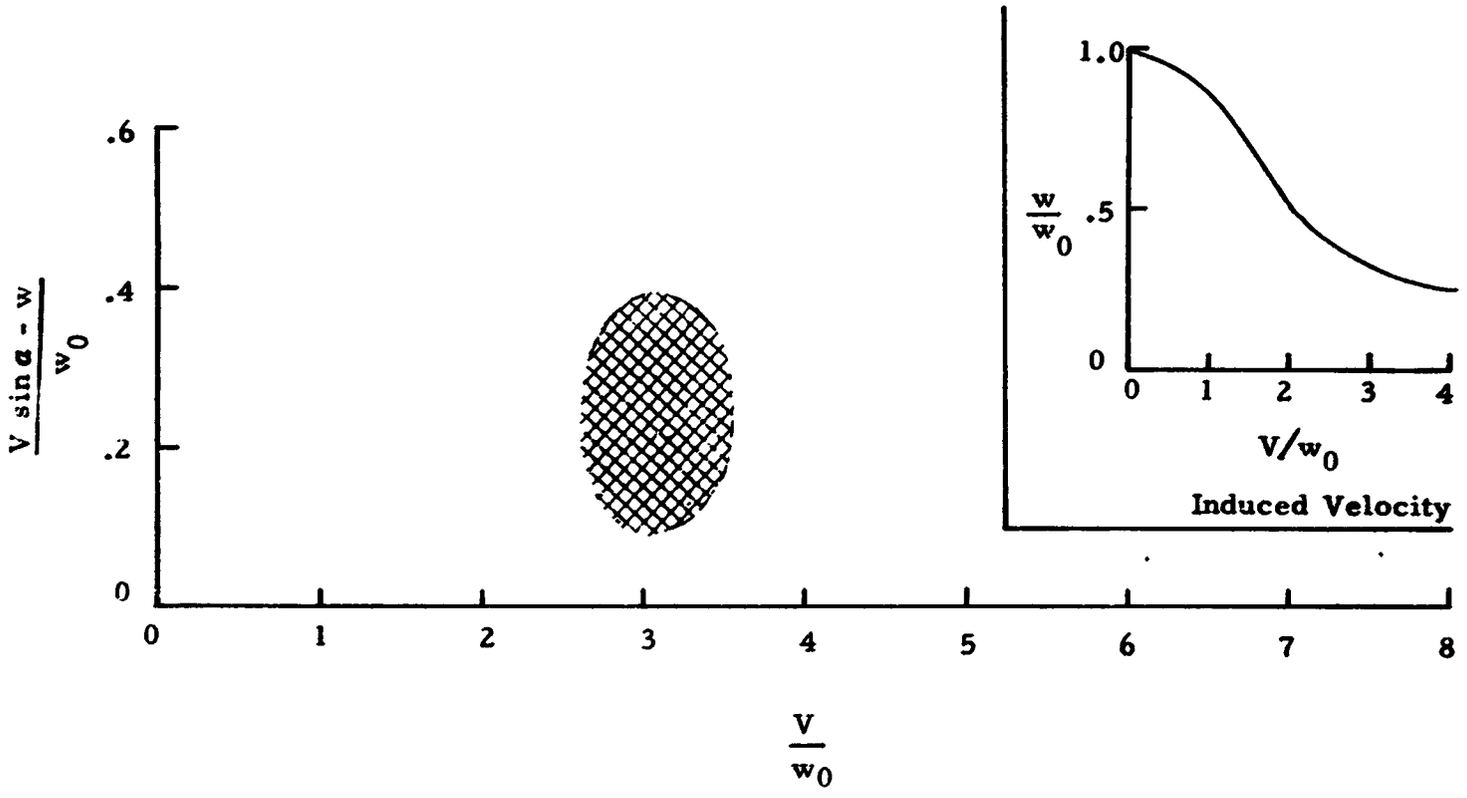

Figure 18. Non-dimensional intense impulsive noise boundary. Level flight non-dimensional induced velocity relationship is also shown.

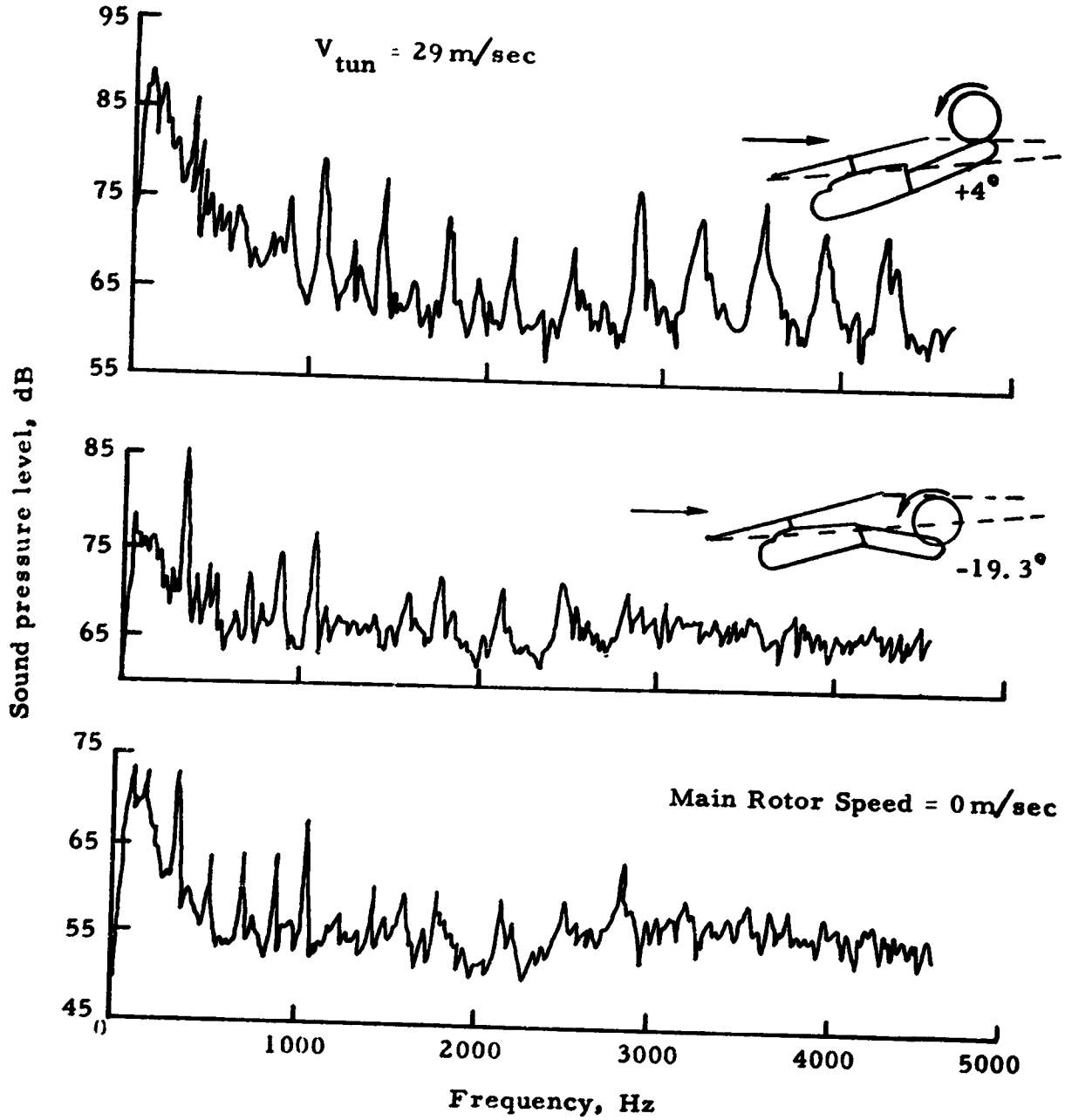

Figure 19. Effect of tail rotor position on noise.

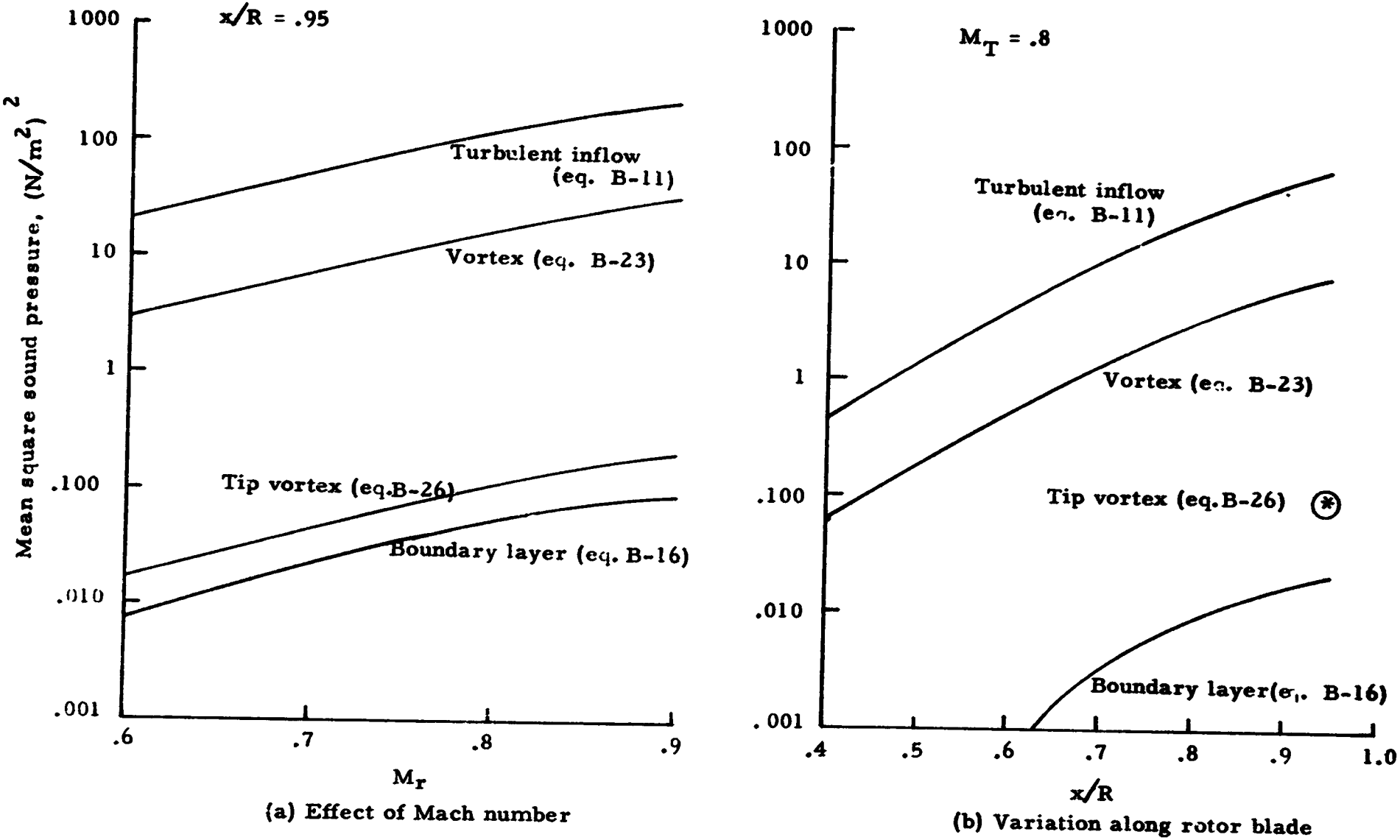

Figure 20. Variation of broadband noise with Mach number and along rotor blade.

APPENDIX A

PERIODIC NOISE

Rotational Noise

The contribution to rotor and propeller discrete noise produced by rotating blade forces (thrust, torque, coning) is called rotational noise. This noise is generated by both the azimuthally uniform steady and nonuniform (periodic) forces acting on the blades. Because the nonuniform blade forces are harmonic in nature, they are frequently referred to as blade-loading harmonics. These forces are the source strength of the acoustic dipole portion of the solution to the wave equation. Rotation of the blades produces movement successively toward and away from the observer, thus introducing effects due to a varying Doppler frequency shift. This modulated Doppler effect causes each loading harmonic to produce more than one sound harmonic in the stationary system. The level of each sound harmonic is thereby the result of the contribution of many loading harmonics. The periodic repetition of these forces at multiples of the blade passage frequency results in a discrete frequency acoustic spectrum.

The analytical approach presented in this report is based on the well-known compact source theory. In recent years, more sophisticated theories for rotating blade noise from noncompact source distributions have been developed. These latter theories require extensive computer capability and will not be treated in this report.

Steady loading theory.- The earliest attempt to formulate a theory of propeller acoustic radiation appears to be that of Lynam and Webb (ref. 16), who recognized that the rotating blades would cause both a periodic modulation of the flow through the disk and a corresponding acoustic disturbance at large distances. Lynam and Webb modeled the action of the blades by a continuous ring of stationary sources and another ring of sinks, with an arbitrary axial displacement; and alternative approach was tried by Bryan (ref. 17) who sought a solution for the sound field of a point source in circular motion. Bryan's paper is interesting as an early, though unsuccessful, example of the retarded-time approach.

Neither of these papers predicted the absolute amplitude for the radiated sound, and it was left for Gutin (ref. 18) to show that, within the frame work of linear acoustics, the steady aerodynamic forces on the rotating blades could be represented by acoustic doublets which are a function of the torque and thrust of the rotating blades. This development is limited to a hovering helicopter rotor, and the approximations limit the accuracy of the calculations of noise to the fundamental and first few harmonics in the far field. Gutin's formulation for the rotational noise is given by equation (A-1)

$$|P_m| = \frac{mB\Omega}{2\pi c_o r} \left| T \cos\theta_1 - \frac{Q}{M_e R_e} \right| J_{mB}(mB M_e \sin\theta_1) \qquad \text{(A-1)}$$

A comparison between the theoretical results given by this method and experimental data for a hovering helicopter rotor (ref. 19) is shown

in figure 12. The comparison in figure 12 is typical, in that Gutin's approach is usually accurate in predicting the fundamental blade passage frequency sound pressure, but underestimates higher harmonic sound pressures. The Gutin theory, using steady loads as inputs, is useful for predicting the low-order pressure harmonics that are most significant for structural problems, but is not adequate for predicting the higher order pressure harmonics that are most significant for subjective reaction.

Gutin's work was extended by Hubbard and Regier (ref. 20) to determine the amplitude and directivity at points as close as one-chord-width from a propeller tip. Several parameters were analytically investigated, and comparisons between theory and experiment were shown to be adequate for tip Mach numbers less than one. Garrick and Watkins (ref. 21) further extended Gutin's theory to include the effects of forward axial speed (vertical climb condition). They synthesized the sound field using the pressure field of a concentrated force moving uniformly at subsonic speeds. The sound field is given in terms of an integral over the rotor disk and, using a simplifying assumption, over an effective ring. Each integral gives expressions for both the near-field and the far-field sound. The effective ring expression for the far-field case (eq. (38) in ref. 21) is:

$$|P_m| = \frac{mB\Omega}{2\pi c_o r \beta_o} \left| \frac{T}{\beta_o^2}\left(M_F + \frac{\cos\theta_1}{\beta_o}\right) - \frac{Q}{M_e R_e} \right| J_{mB}\left(\frac{mBM_e \sin\theta_1}{\beta_o}\right) \qquad \text{(A-2)}$$

Results from equation (A-2) for typical cases show that the direction of maximum noise shifts rearward as forward speed is increased.

Watkins and Durling (ref. 22) extended the work of Garrick and Watkins to demonstrate the importance of spanwise and chordwise load distribution on the harmonic distribution as well as on the overall noise levels. The effect of the chordwise loading distribution is of primary importance.

Figure 13 presents a comparison of typical measured and calculated rotational noise spectra based on a measured 40 percent chordwise-integrated, differential blade-loading spectrum and three different assumed chordwise-loading distributions (ref. 23). It can be seen that all of the distributions provide similar agreement at low frequencies; however, as the harmonic number increases the results begin to diverge. In a majority of case studies, the point loading distribution provided the best agreement between calculation and measurement. The rectangular distribution always provided poor agreement while the sawtooth distribution (which should be a more realistic distribution) provided better agreement. The exact shape of the chordwise-loading distribution is particularly important at frequencies where compact source assumptions begin to break down. However, in most of the cases studied, this assumption was not violated and the point loading distribution was adequate. The generally good agreement between the measured and calculated rotational noise, based on loading measured at eighty percent span, suggests that the aerodynamic loading is representative of the entire rotor.

Unsteady loading theory.- A technique for obtaining solutions to the rotational noise problem when the blade loads are unsteady was advanced by Schlegel, King, and Mull in reference 11. This technique resulted in a

numerically integrated solution which accounted for nonuniform spanwise pressure distributions on the blade. Their chordwise pressure distribution was a rectangular pulse whose amplitude depends on the rotation angle Ωt. Better correlation with experimental data is obtained with this analysis than with that of Gutin. The basic limitation to this solution is that higher harmonic loading data ($m > 30$) were not available. A similar solution was presented by Sadler and Loewy (ref. 24).

The rotational noise analysis of Wright (ref. 25) yields a far-field sound pressure relation which is based on both steady and fluctuating thrust and torque values in a manner similar to that of reference 11. Blade loading is assumed concentrated at one radial position. This analysis provides excellent insight into the modal development of rotational noise and a good basic understanding of the mechanism of noise generation due to a rotational pressure field.

The more widely used prediction technique for rotational noise is that derived by Lowson (ref. 26). He showed that the far-field sound of a point force in arbitrary motion was given by:

$$p = \frac{x_i - y_i}{4\pi c_0 r(1-M_r)^2} \left[\frac{\partial F_i}{\partial t} + \frac{F_i}{1-M_r}\frac{\partial M_r}{\partial t}\right] \qquad \text{(A-3)}$$

where F_i represents the components of the point force, and M_r is the component of the relative Mach number in the direction of the observer. Observer and source locations are x_i and y_i, respectively, and terms like $x_i F_i$ are inner products. Based on equation (A-3) a technique was developed for calculating the rotational noise, using the rotor

thrust, the drag and radial components of blade loading, and a compact source model. The effect of unsteady loads and the hub convection Mach number transformation was included also. In this method, rotor loading harmonics are assumed to decay as inverse functions (λ^{-n}) of the loading harmonic number λ. The exponent n is determined empirically. In addition, the phase between the loading harmonics has been randomized to simplify the calculation procedures, that is, loading harmonic pressures are added in the mean-squared sense.

Equation (A-3) is the basis for the rotational noise equations which are used in the Recommended Prediction Procedures section of this report. The equations used here have been derived in reference 1 as described below.

The complex sound pressure due to the first Λ loading harmonics:

$$\frac{P_m}{\rho c_o^2} = \frac{i^{-m}}{4\pi}\left(\frac{R}{r}\right)\sum_{\lambda=-\Lambda}^{\Lambda} i^{\lambda}\left\{\frac{imM_e(x/r)}{(1-M_r)^2}\left(\frac{C_{\lambda,T}}{\rho c_o^2 R^2}\right)J_{(m-\lambda)}\left[\frac{mM_e(y/r)}{1-M_r}\right]\right.$$

$$-\frac{i}{1-M_r}\left(\frac{C_{\lambda,D}}{\rho c_o^2 R^2}\right)(m-\lambda)\,J_{(m-\lambda)}\left[\frac{mM_e(y/r)}{1-M_r}\right]$$

$$\left.+\frac{mM_e(y/r)}{(1-M_r)^2}\left(\frac{C_{\lambda,C}}{\rho c_o^2 R^2}\right)J_{(m-\lambda)}\left[\frac{mM_e(y/r)}{1-M_r}\right]\right\} \qquad \text{(A-4a)}$$

The mean-squared pressures due to the higher loading harmonics are:

$$P_{m_T}^2 = \frac{1}{2}\left[\frac{1}{2}\left(\frac{R}{r}\right)\frac{mM_e(x/r)}{(1-M_r)^2}\frac{C_{o,T}}{\rho c_o^2 R^2}\right]^2 \sum_{\lambda=\Lambda+1}^{\Lambda_{limit}} \lambda^{-2n_T} J^2_{(m-\lambda)}\left[\frac{mM_e(y/r)}{1-M_r}\right]$$

$$+ \sum_{\lambda=\Lambda+1}^{\Lambda_{limit}} \lambda^{-2n_T} J^2_{(m+\lambda)} \frac{mM_e(y/r)}{1-M_r} \qquad \text{(A-4b)}$$

$$P^2_{m_D} = \frac{1}{2}\left[\frac{1}{2\pi}\left(\frac{R}{r}\right)\frac{mM_e(y/r)}{(1-M_r)}\left(\frac{C_{o,D}}{\rho\, c_o^2 R^2}\right)\right]^2 \left\{ \sum_{\lambda=\Lambda+1}^{\Lambda_{limit}} \lambda^{-2n_D}(m-\lambda)^2 J^2_{(m-\lambda)} \frac{mM_e(y/r)}{1-M_r} \right.$$

$$\left. + \sum_{\lambda=\Lambda+1}^{\Lambda_{limit}} \lambda^{-2n_D}(m+\lambda)^2 J^2_{(m+\lambda)} \left[\frac{mM_e(y/r)}{1-M_r}\right] \right\} \qquad \text{(A-4c)}$$

and

$$P^2_{m_C} = \frac{1}{2}\left[\frac{1}{2\pi}\left(\frac{R}{r}\right)\frac{mM_e(y/r)}{(1-M_r)^2}\left(\frac{C_{o,C}}{\rho\, c_o^2 R^2}\right)\right]^2 \left\{ \sum_{\lambda=\Lambda+1}^{\Lambda_{limit}} \lambda^{-2n_C} J^2_{(m-\lambda)} \left[\frac{mM_e(y/r)}{1-M_r}\right] \right.$$

$$\left. + \sum_{\lambda=\Lambda+1}^{\Lambda_{limit}} \lambda^{-2n_C} J^2_{(m+\lambda)} \left[\frac{mM_e(y/r)}{1-M_r}\right] \right\} \qquad \text{(A-4d)}$$

Equations (A-4a) through)A-4d) are then added in a mean-squared sense

$$P^2_m = P^2_{m_{\lambda\leq\Lambda}} + P^2_{m_{T\ \lambda>\Lambda}} + P^2_{m_{D\ \lambda>\Lambda}} + P^2_{m_{C\ \lambda>\Lambda}} \qquad \text{(A-5)}$$

The unsteady forces acting on a rotor blade come from many mechanisms; rotor/rotor wake interaction, atmospheric turbulence, blade motion, and airfoil characteristics, among others. An analytical method that can accurately predict the combined effect of all the sources mentioned above is still beyond the present state-of-the-art.

In their studies, Lowson and Ollerhead (refs. 3, 27) noted that measured blade airloading harmonic amplitudes tended to fit an exponential decay relation with harmonic number. This takes the form:

$$C_\lambda = C_0 \lambda^{-n} \qquad \text{(A-6)}$$

where C_0 is the amplitude of the first harmonic, λ is the loading harmonic number, and n is the decay exponent. The loading decay rate for a given configuration will vary with the type of flight and atmospheric conditions. Increased high frequency airloads can be expected to have more effect on the higher order sound harmonics than the lower order ones. Unfortunately, very little experimental data are available beyond the 10th airloading harmonic so that the airloading harmonic spectrum is far from being completely defined. Reference 2 gives a review of existing data on loading decay rates for a variety of operating conditions and rotors.

Lowson and Ollerhead (ref. 3) have shown that loading harmonics of order λ are significant radiators into the m^{th} sound harmonic in the range:

$$mB\,(1-M) < \lambda < mB\,(1+M) \qquad \text{(A-7)}$$

It has been determined by Sternfeld et al (ref. 28) that phase differences between the lower loading harmonics were of importance. Since precise harmonic phasing of the airloads cannot be determined (being to a large extent a function of random factors), the logical approximation is to assume that each loading harmonic is randomly phased with respect

to the others. Since this assumption is not necessarily true for a specific situation, relative phasing error between loading harmonics could account for the random phasing, Lowson (ref. 3) adjusted the loading exponent by adding .5. Hosier's data (ref. 23) substantiates random phasing in a band $\pm$ 40 degrees about 0, with the exception of the very lowest harmonics where more precise phase information seems important.

Compressibility-induced profile drag noise.- Periodic blade loading can have a gross effect on the radiated noise of a rotating blade system when the blade speeds are transonic. The sources of these unsteady blade loadings for subsonic blade speeds were discussed in the previous section. This section deals with the periodic blade torque-force fluctuation due to the compressibility associated with high tip speeds. Noise generated by these periodic blade loadings have a tendency to dominate the noise signature of a helicopter when they occur. This is commonly called impulsive noise.

The rotor impulsive noise signature can be characterized by at least six variables which contribute to the overall sharp-slapping or cracking effect. These variables are shown in figure 14. Of the variables shown, crest factor and rise time are considered to be of first order importance. Psychoacoustic investigations currently in progress estimate that the crest factor (ratio of peak pressure to rms pressure) must be greater than 15 dB for the signature to be considered impulsive. Additional information relating to the subjective aspects of helicopter impulsive noise can be found in references 9, 30, and 31 respectively. References 32, 33, and 34 address the problem of providing a rating for helicopter impulsive noise.

There is a substantial increase in the impulsive noise of the rotor as the advancing tip speed goes above Mach 0.7. Since aerodynamic compressibility effects such as the appearance of oscillating shock waves on the blades also become important in this tip speed range, this is called compressibility noise. From the acoustic point of view, the thickness and loading noise also show a similar behavior in both the increase of noise level and the directivity pattern. However, recent studies by Boxwell, Schmitz and Yu and also by Hanson and Fink have shown that the nonlinear effects, resulting from the quadrapole source term in the governing acoustic equation of Ffowcs Williams and Hawkings, may be also important in the calculation of compressibility noise.

The highly directional characteristic of advancing blade impulsive noise can be shown theoretically from Lowson's (ref. 3) equation where the distance to the observer is modified by a Mach number correction. This effect becomes of greater importance with increased harmonic number, and has been identified experimentally by Cox (ref. 31) in full-scale wind-tunnel tests. Results from a recent flight investigation (ref. 35) indicate that at an airspeed of 130 knots, a region on the advancing side of the rotor disk extending from 75 percent radius to the blade tip was experiencing some degree of shock phenomena. Thus, while there is an acoustic source effect at high tip speeds which is partially responsible for the generation of impulsive noise, the advancing blade tip Mach number, which is a function of aircraft forward speed, accounts for the highly directional character of this type of noise. Arndt and Borgman (ref. 6) have presented an expression showing the effect of compressibility drag

on the impulsive noise as:

$$P_{mB} = \frac{mB\,\bar{C}_{d_o}}{4\pi^2\sqrt{2}}\,\frac{\Delta\psi}{\pi}\,\frac{R}{R_e}\,\frac{c}{r}\,\rho c_o^2 \sum_{j=-\infty}^{+\infty} \left(1-\frac{j}{mB}\right)\,\beta_j\,J_{(mB-j)}(mB\,M_e\sin\theta) \qquad \text{(A-8)}$$

Besides aircraft configuration parameters, this expression is also a function of incremental drag coefficient, $\bar{C}_{d_o}$, and the azimuth angle, $\Delta\psi$, over which the Mach number is greater than the drag divergence Mach number, M_{dd}. Figure 15 shows the variation of M_{dd} for typical helicopter airfoil sections. Equation (A-8) was derived from the basic rotational noise equations with only the drag term being considered.

Thickness Noise

Blade thickness noise is due to the volume displacement of the air surrounding the blade, as it moves through the air. This noise is strongly directional in the plane of rotation. Observed sound radiation from helicopters in high speed forward flight suggests that as the blade tip advances a strong pressure pulse is generated. The noise from this source increases rapidly with advancing tip Mach number and becomes considerably stronger than the rotational noise components.

Ernsthausen (refs. 37, 38) using primarily an experimental analysis, studied the characteristics of thickness noise. He emphasized the predominance of higher harmonics at blade tip Mach number near 1.0. Deming (ref. 38) performed experimental and theoretical work with symmetrical blade sections operating at zero angle of attack and developed the first

theory for thickness noise. The development of this theory follows much the same procedures as Gutin's rotational noise work, however, his analysis is essential for noncompact sources. The airfoil is replaced by a distribution of acoustic monopole sources operating next to the infinite wall. The strength of these sources is the normal velocity distribution on the airfoil. Due to the lack of high-speed computers Deming introduced approximations so that the calculations of the fundamental and the first few harmonics are realistic. His calculations are limited to static propellers with the observer in the far field. The Diprose model (ref. 39) for thickness noise considered distributed radial and chordwise blade sources. This model is a slight improvement to the compact source theory. Based on the original work of Billing (ref. 40), Arnoldi (ref. 41) formulated a procedure which includes the near- and far-field thickness noise for compact sources.

More recently, Hawkings and Lowson (ref. 7) presented a theoretical analysis of supersonic rotor noise. This analysis results in a noncompact solution to the Lighthill theory of aerodynamic noise. The solution is relatively tractable once the blade configuration is known. The following equation is valid for hovering conditions:

$$P_{mB} = \frac{4B}{\sqrt{2}\pi} M_T^2 \rho c_o^2 \left(\frac{R}{r}\right)\left(\frac{h}{c}\right) \int_1^\infty \frac{1}{\xi^4}\left(\frac{\sin mB\, k\xi}{mB\, k\xi} - \cos mB\, k\xi\right) J_{mB}\left[\frac{M_r \cos\beta}{\xi}\right] d\xi \qquad \text{(A-9)}$$

The spectrum shape of the thickness noise component is directly affected by the Mach number and the chord-to-diameter (slenderness)

ratio. The spectrum shape is determined by the integral of equation A-9. Figure 16 shows how the variation of these two parameters affects the shape for inplane measurements. Increasing the slenderness ratio (c/D) of the rotor blade does not change the spectrum shape - only the level. Changing the Mach number, however, changes both the shape and sound pressure level. The results of this equation provide reasonable agreement with the more sophisticated theory of Farassat (ref. 42) out to approximately 40 harmonics. Equation (A-9) is used in the Recommended Prediction Procedures section of this report.

Interaction Noise

In this section, the generation of discrete noise due to the impingement or interaction of a trailed line vortex on a following lifting surface will be discussed. Two cases are of considerable importance to aircraft using rotating blade systems: first, the vortex interaction with either a following blade of a helicopter main or tail rotor which generally results in an impulsive noise condition (commonly referred to as blade slap) occurring over selected areas of the flight envelope and second, the installation effects wherein tail rotor inflow or wake are distorted by aircraft geometry.

Blade/vortex interaction.- The generation of lift by a helicopter rotor blade results in a complex aerodynamic flow-field. This flow-field is composed of turbulent air and shed tip vortices. Rapid blade lift fluctuations generated by the interaction of a vortex from another blade will result in impulsive noise. Noises of this type, when they occur, can be predominant. An accurate analysis of this noise is dependent on a

knowledge of the geometry and dynamics of the concentrated shed rotor wake and on the ability to predict the time-variant blade lift distribution.

Two principal types of helicopter interaction noise occur; these are due to vortex-impingement with the following blade and vortex-impingement with the tail rotor. Figure 17 shows, schematically, two orientations of a vortex interacting with a lifting blade. Figure 17(a) shows a vortex with axis parallel to the blade, a situation which represents the most severe case. In this case, the pressure distribution along a large portion of the blade span will undergo a rapid angle-of-attack change which results in an impulsive noise. In figure 17(b), the axis of the vortex core is perpendicular to the blade-span and only a small spanwise section of blade is affected but over a relatively long period of time. The incremental loading experienced by the blade is caused by the induced velocity field of the vortex which forces a change in the blade section angle-of-attack. The magnitude of this angle-of-attack change is directly proportional to the strength of the vortex and inversely proportional to the spacing between blade and vortex.

The influence of the shed main-rotor wake on the noise generated by the tail rotor may be significant in some cases. The primary operating parameters associated with this problem are:

(a) the advance ratio, μ, (the main rotor wake intersects the tail rotor at different azimuth locations because of wake sweep angle),

(b) the direction of tail rotor rotation (under some operating conditions the wake vortex can either increase or decrease the relative tail rotor tip speed),

(c) the tail rotor tip speed, and

(d) the main rotor thrust and associated tip vortex strength (the rotor loading coefficient provides an indication of how fast the wake moves vertically away from the main rotor and consequently where it interacts with the tail rotor).

Accurate calculation of a helicopter vortex wake trajectory is a very complex computational process which can be done only with the aid of a computer. The primary reason for this is the interaction of the vortex filaments with each other. Two such wake programs are currently available and are outlined in references 43 and 44. A less accurate, but still useful, representation of the early stage of a helicopter vortex wake trajectory evolution can be found in reference 45.

In an effort to avoid the previously outlined complications, a technique has been derived to locate the flight region of maximum impulsive noise based on currently available experimental noise data (ref. 46). Figure 1B presents the maximum impulsive noise boundary as a function of two non-dimensional velocities.

The nondimensional velocity variables employed in this presentation are

$$\frac{V\sin\alpha + w}{w_o} \text{ (ordinate)}, \qquad \frac{V}{w_o} \text{ (abscissa)}$$

To convert this nondimensional region to the more familiar rate of descent against airspeed presentations, the flight conditions and rotor loadings must be known. The following equations can be used to perform the conversion:

$$V_d = V \sin \gamma$$

$$\sin \gamma = \sin \alpha - \frac{D_p}{W}$$

$$\sin \alpha = \frac{1}{V} \left(\frac{P}{T} - w\right)$$

$$w_o = \frac{DL}{2\rho}$$

w - from insert in figure 7 taken from reference 47

Although figure 18 identifies the flight region where the maximum impulsive noise can be expected, the magnitude of the noise is dependent on the helicopter configuration. The calculation of the blade/vortex interaction impulsive noise will be discussed next.

Various researchers have investigated the far-field noise resulting from a blade-vortex interaction. Notable among this research is that of Leverton (ref. 48), Widnall (ref. 49) Padakannaya (ref. 50), Filotas (ref. 51), and Wright (ref. 25). Leverton's acoustic analysis is based on Lighthill's formulation for far-field sound pressure where the loading on a small area of the blade can be assumed to act as a point dipole acoustic source (chord assumed smaller than wave-length). Widnall models the interaction as a two-dimensional airfoil an an oblique gust. The analysis was extended to interaction at the tip region where the effects of unsteady aerodynamics must be accounted for. However, in both techniques, the radiated noise is determined by the rate-of-change of the blade force. Padakannaya (ref. 50) utilized a more flexible vortex-lattice method for the calculation on the unsteady airloads. Reasonably

good correlation between experimental and calculated data was shown in this work. Filotas (ref. 51) derives a sound pressure expression by modeling a finite aspect ratio wing flying at a uniform speed over a carpet of equally spaced, infinitely long lines of vortices. Using the method developed by Wright (ref. 8), an equation for the harmonic sound pressure level has been derived. This equation is dependent on a Fourier representation of a sinusoidal blade loading occurring once per revolution. The prediction method used in this report is based on the following formulation by Wright:

$$P_{mB} = \left(\frac{\Delta L}{L_o} E\rho_w\right) K_T\, mB\, X_s \qquad \text{(A-10)}$$

where E is the number of interactions occurring every revolution, ρ_w is the load solidity or the fraction of the effective disk annulus that the unsteady loading region occupies, K_T is a thrust constant and X_s is the blade loading spectrum function.

A research program using small rotors in a static operating situation (ref. 52) revealed the effect of configuration on the shed vortex characteristics. It was found during this investigation that an increase in the number of blades reduced the axial spacing between vortices and increased the angular rate at which they revolve about their centroids of vorticity, which caused them to become more unstable and to diffuse sooner.

The effect of collective pitch on vortex strength is that axial spacing between vortices decreases along with vortex strength. The tip vortices become increasiggly unstable and diffuse more rapidly. It was

observed (ref. 52) that the effect of tip speed on vortex trajectory was generally not noticed but that unstable sinusoidal fluctuations occur close to the rotor once a strong shock wave forms on the surface of the airfoil. This instability was noticed at Mach numbers above .75 for a NACA 0012 airfoil.

Installation effects.- Rotor noise due to installation effects generally results from the interaction of the rotor wake interaction with fuselage, wing, nacelle, tail fin, or another rotor. The basic mechanisms that alter the rotational noise due to distorted inflow have been previously discussed in the Unsteady Loading Theory section. In the case of pusher tail rotor configuration (rotor thrust vector toward fin, inflow over fin) the turbulent wakes from the tail fin can give rise to a severely distorted inflow which significantly increases the noise generated. This occurs in a manner similar to the rotor-stator interaction phenomenon (ref. 53) which exists in turbofan engines. This unsteady fin force has been measured on a full-scale helicopter in reference 54. The effect of interaction of the main rotor wake on the blade loading of a tail rotor was investigated in model studies in reference 55. It was noted in this experiment that the main rotor wake impingement location on the tail rotor produced increased tone noise at tail rotor blade passage frequency and produced the occurrence of combination tones, i.e., tones which are a function of both the main and tail rotor rotational frequency. Figure 19 presents acoustic spectra to 5000 Hz and shows the effect of wake location on the tail rotor noise.

APPENDIX B

BROADBAND NOISE

Initial investigation into the basic mechanisms of isolated airfoil noise was guided by Sharland (ref. 56) and Curle (ref. 57). He suggested that broadband noise from a surface in a moving flow can be described by at least three mechanisms which cause random fluctuating forces. One form of random fluctuating force is the surface pressure field arising from a turbulent boundary layer. Another form is the force fluctuations resulting from shed vorticity. Finally, if the surface is moving in a flow which is initially turbulent, a third component of fluctuating force can arise. Once the mechanisms of noise generation are postulated in a physical sense, analytical models can be derived to indicate how much acoustic power is generated from each source mechanism and which parameters affect the source strength. A detailed discussion of these mechanisms is contained in reference 58 and is summarized next. The relative importance of the various broadband noise sources are then presented in summary figure for a typical helicopter rotor blade. The sound pressures were calculated along the rotating blade at 10 equal blade areas.

Inflow Turbulence Noise

This section will outline the radiation from a plate in a turbulent airflow. If the speed is subsonic, the acoustic wavelength will be larger than the turbulence scale so that sound from plates of dimensions up to several times the turbulent scale should be calculated simply

from the fluctuating pressures. The expression for the fluctuating density from a distribution of fluctuating sources can be written as

$$\rho = \frac{x_i - y_i}{4\pi c_o^3 r^2} \int_A \frac{\partial p_i}{\partial t} \, dA \qquad \text{(B-1)}$$

The total acoustic power, W, is the integral of $\frac{c_o^3 \rho^2}{\rho_o}$ over the field which is

$$W = \frac{1}{12\pi\rho c_o^3} \int_A \int_A \frac{\partial p(x)}{\partial t} \frac{\partial p(x')}{\partial t} \, dA dA' \qquad \text{(B-2)}$$

The retarded source time correlation of the rate-of-change of pressure on the plate must now be evaluated. To obtain equation (B-7) it has been assumed that the plate dimension was of the order of the acoustic wavelength. If it is assumed that this dimension is small compared to the wavelength then the "compact" source assumption can be utilized and the retarded time assumption dropped. One of the integrations over the surface is simply a correlation integral which can be written:

$$\int_{A'} \frac{p(x)}{\partial t} \frac{\partial p(x')}{\partial t} \, dA' = \frac{\partial p}{\partial t}^2 A_c \qquad \text{(B-3)}$$

where A_c is the correlation area of the pressures. Substituting equation (B-3) into equation (B-2) gives:

$$w = \frac{1}{12\pi\rho c_o^3} \int_{A_b} \frac{\partial p}{\partial t}^2 A_c \, dA_b \qquad \text{(B-4)}$$

If the blade is in a homogeneous path of turbulence, then the integral simply becomes a multiple of the blade area, A_b. To evaluate equation (B-4) for the case of impinging turbulence we may take advantage of the results of Kemp and Sears (ref. 59) as simplified by Lowson (ref. 58). This shows that the mean lift per unit span, L, on an airfoil in a sinusoidal gust of frequency, ω, and magnitude, u, is

$$L = \frac{\pi\rho c\, Uu}{\left(\frac{\pi\omega c}{U}\right)^{1/2}} \tag{B-5}$$

where c, is the airfoil chord. To extend this to three dimensional conditions we note that the mean lift in terms of pressure fluctuations is

$$L = p_{rms}\,(\ell_c c)^{1/2} \tag{B-6}$$

where ℓ_c is the correlation length in the chordwise direction. Let

$$\frac{\partial p}{\partial t}^2 = \omega^2 p_{rms}^2 \tag{B-7}$$

where ω is a typical frequency, then equation (B-4) becomes

$$w = \frac{1}{12\pi\rho c_o^3} A_c\,(2A)\,\frac{\omega^2}{\ell_c c}\,\frac{\pi\rho c U^3 u^2}{\omega} \tag{B-8}$$

The 2A arises because both sides of the plate radiate. Put

$$\omega = \frac{U}{\ell} \tag{B-9}$$

where ℓ is a typical length and let $A_c = \ell^2$, $\ell_c = \ell$ and $A = A_b$,

the final result for the sound power radiated from an airfoil due to incident turbulence is

$$W = \frac{1}{6} \rho c_o^3 M^6 \left(\frac{u}{U}\right)^2 A_b \qquad \text{(B-10)}$$

$$(SP)^2 = \frac{\rho^2 c^4}{24\pi r^2} M^6 \left(\frac{u}{U}\right)^2 A_b \qquad \text{(B-11)}$$

Equation (B-11) has been plotted in figure 19 as a function of Mach number for a typical helicopter blade. Brown and Ollerhead (ref. 60) provide an approximation to the maximum wake turbulence in terms of the lifting surface parameters:

$$\frac{u}{U} = .1 \left[1 - \left(1 - \frac{2.42 \, \bar{c}_{d_o}^{1/2}}{.3} \right)^{1/2} \right]^{1/2} \qquad \text{(B-12)}$$

This result is similar to that of Sharland (ref. 56) for the same case. The typical frequency for turbulence-induced noise will vary as the frequency content of the turbulence that is interacting with the surfaces.

Boundary Layer Noise

The same general formula, equation (B-5), can be applied to radiation from the boundary layer pressure fluctuations acting on the plate. Although theory indicates that the direct quadrupole radiation from the turbulence is stronger for this case, it is of interest to attempt a boundary layer pressure fluctuation calculations. Equation (B-4) can be written as

$$W = \frac{1}{12\pi \rho c_o^3} \int p^2 {}^2A_c dA \qquad \text{(B-13)}$$

Experiments indicate that p^2 is of the order of $36 \times 10^{-6}\, q^2$, where q is the dynamic head ($\frac{1}{2}\rho U^2$). However, there is less agreement over the magnitudes of the correlation data. Values of correlation areas assumed by various authors are given in Table I.

TABLE I

Pressure Correlation Areas in a Turbulent Boundary Layer

Source	A_c	δ^*	$\omega^2 A_c$
Doak	$144.00\delta^{*2}$	$0.63\ U/\omega$	$58.000\ U^2$
Lighthill	$4.40\delta^{*2}$	$0.05\ U/\omega$	$0.011\ U^2$
Bull and Willis	$1.78\delta^{*2}$		
Sharland			$0.500\ U^2$
Bull	$1.50\delta^{*2}$	$0.30\ U/\omega$	$0.135\ U^2$

Most recent studies of boundary layer pressure fluctuations have broadly agreed with Bull's data, (ref. 61). Therefore, the correlation area can be given by the expression

$$\omega^2 A_c = K_1 U^2 \qquad \text{(B-14)}$$

where the constant K_1 is in the range $0.1 < K_1 < 1.0$. Substitu ting equation (B-14) into (B-13) yields the approximate result.

$$W = \frac{9\,K_1}{12}\,\rho\,c_o^{\,3}\,M^6\,A \times 10^{-6} \qquad \text{(B-15)}$$

or the sound pressure:

$$(SP)^2 = \frac{9\,K_1}{48^2}\,\rho^2 c_o^{\,4}\,M^6\,\frac{A}{r^2} \times 10^{-6} \qquad \text{(B-16)}$$

Equation (B-16) is shown in figure 20 in comparison with the other broadband noise source components. The effect of boundary layer noise is of second order importance when compared to the other sources. Equation (B-15) is in agreement with Sharland (ref. 56).

Vortex Noise

The vortex noise source can be categorized into two components. The first component results from lift fluctuations produced at the trailing edge of the blade by shed vortices, and the second component occurs when a tip vortex interacts with a blade tip. An alternate approach to the determination of vortex noise has been presented by Lowson in reference 9. This approach is based on a dimensional dependence of sound from fluctuating forces.

Presented below are the relationships for vortex shedding noise as hypothesized by Sharland (ref. 56) and tip vortex self-interaction noise as stated by Lowson (ref. 58).

Vortex shedding.- Beginning with equation (B-4), an expression can be derived for the total radiated power due to vortex shedding. If we think of the fluctuating pressure difference as a local lift fluctuation

per unit area, then p can be expressed in terms of the local lift coefficient C_l

$$p = \frac{1}{2} \rho U^2 C_L \tag{B-17}$$

Where U is the local mean velocity parallel to the surface. Therefore,

$$\frac{\partial p}{\partial t} = \frac{1}{2} \rho U^2 \frac{\partial C_L}{\partial t} \tag{B-18}$$

and

$$W = \frac{\rho}{48\pi c_o^3} \int U^4 \left(\frac{\partial C_L}{\partial t} \right)^2 A_c dA \tag{B-19}$$

In order to describe the integral in equation (B-19) in terms of the flow parameters the mechanisms by which lift fluctuations are produced in the absence of external excitation must be known. There is still some uncertainty about the magnitude of lift fluctuations induced by the bound circulation changes which accompany trailing edge vortex shedding, but it has been suggested that the lift fluctuations can be related to time fluctuations in the boundary layer thickness at the trailing edge. On this basis, for conditions typical of propeller blades, the root mean square of the fluctuating lift coefficient should be of the numerical order of the -1/5 power of the Reynolds number. The frequency of the lift fluctuations should be about the same as the characteristic frequency of vortex shedding at the trailing edge:

$$\omega = 2\pi f = \frac{4\pi U}{c} \tag{B-20}$$

where c is the chord. For instance, a rotating blade with a 10-percent thickness ratio, the correlation area should be governed by the size of the larger eddies at the trailing edge, which might be on the order of half the section thickness, that is $.05c^2$. Equation (B-19) can be rewritten as

$$W = \frac{\rho}{48\pi c_o^3} \int_A U^4 \omega c_L^2 A_c dA \qquad \text{(B-21)}$$

or integrating,

$$W = \frac{\pi\rho U^6 (RN)^{-.4} A}{120 c_o^3} = \frac{\pi}{120} \rho c_o^3 M^6 (RN)^{-.4} A \qquad \text{(B-22)}$$

A typical sound pressure level assuming a dipole distribution is

$$(SP)^2 = \frac{1}{480} \rho^2 c_o^4 \frac{A}{r^2} M^6 (RN)^{-.4} \qquad \text{(B-23)}$$

Tip radiation.- Utilizing the previously derived equation for turbulence induced noise (eq. B-10)) and assuming that correlation lengths are on the order of 5 percent of the chord, a typical frequency is

$$\omega = 40 \frac{U}{c} \qquad \text{(B-24)}$$

then substituting into equation (B-17)

$$W = \frac{3}{\pi} \frac{\rho}{c_o^3} U^6 A_T \times 10^{-6} = \frac{3}{\pi} \rho c_o^3 M^6 A_T 10^{-6} \qquad \text{(B-25)}$$

where A_T is the blade tip area over which the vortex interaction is to occur. This area is assumed to be approximately 5 percent of the blade area. If a dipole distribution is assumed, then the sound pressure is

$$(SP)^2 = \frac{3}{4\pi^2} \frac{\rho^2 c_o^4}{r^2} M^6 A_T \times 10^{-6} \qquad \text{(B-26)}$$

Recent work presented by Clark (ref. 62) indicates that when blade tip twist is used on a helicopter rotor a pronounced reduction in noise level is evident. One effect of tip twist is to modify the blade tip vortex.

The four broadband noise sources; turbulent (eq. B-11)), a vortex (eq. (B-23)), tip radiation (eq. (B-26)), and boundary layer (eq. (B-16)), are compared in figure 20. This figure shows the calculated variation of these noise sources with rotor tip Mach number and rotor radius. From figure 20(a), the predominant noise source is that resulting from turbulent inflow. The shed vortex noise source is the second source of importance. The broadband noise from the boundary layer and vortex impingement on the tip are insignificant. Figure 20(b) shows the variation of the various broadband noise sources along the rotor radius. The primary broadband noise radiation portion of the rotor blade seems to be the outboard 50 percent.

Dimensional dependence of sound from fluctuating forces.- Early work on broadband noise performed by Yudin (ref. 63) and later modified by Hubbard (ref.10) and Schlegel (ref.11) assumed explicitly that the sound generation was due to trailing edge vortex effects. This work was based primarily on dimensional arguments. The method developed in this

section has been correlated with measured broadband noise from helicopter rotor blades and is in reasonable agreement. For a point fluctuating force the basic law governing the sound radiation is well known (Curle, ref. 57) as

$$p \sim \frac{\partial F}{\partial t} \tag{B-27}$$

To calculate the sound radiated by a random pressure field acting over an area, it is necessary to split up the field into correlation areas A_c over which the pressure may be regarded as coherent. Thus, the equivalent point force is given by $F = A_c P$. Because the force is random the overall sound pressure is given by the sum of the square of the effects of the random forces. Thus, if there are E individual events over the blade the total mean square sound pressure is given by

$$(SP)^2 \sim E\, A_c^{\,2} \left(\frac{\partial p}{\partial t}\right)^2 \tag{B-28}$$

It is usual to assume that the magnitude of the fluctuating pressures acting on the blade is simply proportional to the mean pressure, that is to the mean thrust divided by the blade area A_b,

$$(SP)^2 \sim k(f)\ \frac{A_c\, f^2\, T^2}{A_b} \tag{B-29}$$

where f is a typical frequency for the fluctuating forces. In turn, f may be put proportional to a typical velocity divided by a typical length, ℓ, thus giving

$$(SP)^2 \sim \left(\frac{A_c}{2}\right) \frac{V^2 T^2}{A_b} \qquad \text{(B-30)}$$

The dimensional dependence on $V^2 T^2 A_b^{-1}$ has been used in several data collapses, and forms the basis for the recommended prediction procedure for helicopter rotor broadband noise used in this report. The spectral features of the broadband noise are distinctly similar in all cases. It would appear to define a "universal" spectral distribution for the broadband noise and to relate the center frequency to the aircraft's operating parameters. This has been done by Munch (ref. 12).

The sound pressure level of a third octave band of rotor broadband noise is

$$SPL_{1/3} = 20 \log \left(\frac{V_T}{c_o}\right)^3 + 10 \log \frac{A_b}{r^2} (\cos^2 \theta_1 + .1) + S_{1/3} + f(\bar{C}_L) + 130 \qquad \text{(B-31)}$$

where $10 \log(\cos^2\theta_1 + .1)$ is the directionality effect as derived by Lowson (ref. 9). The generalized empirical spectrum shape number, $S_{1/3}$, is shown in figure 20. Data collapses were performed using measured rotor data to provide this spectrum shape. The peak frequency was determined to be

$$f_p = -240 \log T + 2.448 V_T + 942 \qquad \text{(SI units)(B-32a)}$$

$$f_p = -240 \log T + .746 V_T + 786 \qquad \text{(English units)(B-32b)}$$

The effect of mean rotor lift coefficient has been based on the initial derivation of equation (B-31) and empirical flight information. Broadband noise increases rapidly with mean lift coefficients greater than approximately .48. The lift coefficient function, $f(\bar{C}_L)$, is defined below as:

$$f(\bar{C}_L) = \begin{cases} 10 \log \frac{\bar{C}_L}{.4} & \text{for } \bar{C}_L \leq .48 \\ .8 + 80 \log \frac{\bar{C}_L}{.48} & \text{for } \bar{C}_L \geq .48 \end{cases}$$

Sound pressure levels for rotors with mean lift coefficients much greater than .6 have not been rigorously verified. Practical helicopter flight conditions, however, generally have lift coefficients less than .6.